Astronomy & Astrophysics

Laboratory spectroscopic study and astronomical detection of vibrationally excited *n*-propyl cyanide

Holger S. P. Müller[1], Adam Walters[2,3], Nadine Wehres[1], Arnaud Belloche[4], Olivia H. Wilkins[1],
Delong Liu (刘德龙)[2,3], Rémi Vicente[2,3], Robin T. Garrod[5], Karl M. Menten[4],
Frank Lewen[1], and Stephan Schlemmer[1]

[1] I. Physikalisches Institut, Universität zu Köln, Zülpicher Str. 77, 50937 Köln, Germany
   e-mail: hspm@ph1.uni-koeln.de
[2] Université de Toulouse 3, OMP, IRAP, 31028 Toulouse, France
[3] CNRS, IRAP, 9 Av. Colonel Roche, BP 44346, 31028 Toulouse Cedex 4, France
[4] Max-Planck-Institut für Radioastronomie, Auf dem Hügel 69, 53121 Bonn, Germany
[5] Departments of Chemistry and Astronomy, University of Virginia, Charlottesville, VA 22904, USA

ABSTRACT

Context. We performed a spectral line survey called Exploring Molecular Complexity with ALMA (EMoCA) toward Sagittarius B2(N) between 84.1 and 114.4 GHz with the Atacama Large Millimeter/submillimeter Array (ALMA) in its Cycles 0 and 1. We determined line intensities of *n*-propyl cyanide in the ground vibrational states of its *gauche* and *anti* conformers toward the hot molecular core Sagittarius B2(N2) which suggest that we should also be able to detect transitions pertaining to excited vibrational states.

Aims. We wanted to determine spectroscopic parameters of low-lying vibrational states of both conformers of *n*-propyl cyanide to search for them in our ALMA data.

Methods. We recorded laboratory rotational spectra of *n*-propyl cyanide in two spectral windows between 36 and 127 GHz. We searched for emission lines produced by these states in the ALMA spectrum of Sagittarius B2(N2). We modeled their emission and the emission of the ground vibrational states assuming local thermodynamic equilibrium (LTE).

Results. We have made extensive assignments of *a*- and *b*-type transitions of the four lowest vibrational states of the *gauche* conformer which reach J and K_a quantum numbers of 65 and 20, respectively. We assigned mostly *a*-type transitions for the *anti* conformer with J and K_a quantum numbers up to 48 and 24, respectively. Rotational and Fermi perturbations between two *anti* states allowed us to determine their energy difference. The resulting spectroscopic parameters enabled us to identify transitions of all four vibrational states of each conformer in our ALMA data. The emission features of all states, including the ground vibrational state, are well-reproduced with the same LTE modeling parameters, which gives us confidence in the reliability of the identifications, even for the states with only one clearly detected line.

Conclusions. Emission features pertaining to the highest excited vibrational states of *n*-propyl cyanide reported in this work have been identified just barely in our present ALMA data. Features of even higher excited vibrational states may become observable in future, more sensitive ALMA spectra to the extent that the confusion limit will not have been reached. The ^{13}C isotopomers of this molecule are expected to be near the noise floor of our present ALMA data. We estimate that transitions of vibrationally excited *iso*-propyl cyanide or aminoacetonitrile, for example, are near the noise floor of our current data as well.

Key words. astrochemistry – line: identification – molecular data – radio lines: ISM – ISM: molecules – ISM: individual objects: Sagittarius B2(N)

1. Introduction

Radio astronomical observations of the warm (>100 K) and dense parts of star-forming regions known as hot cores or hot corinos have revealed a wealth of complex molecules. These are, for the most part, saturated or nearly saturated with up to 12 atoms thus far (Belloche et al. 2014). Details can be found on the Molecules in Space web page[1] of the Cologne Database for Molecular Spectroscopy, CDMS (Müller et al. 2001, 2005) or on the list of Interstellar & Circumstellar Molecules[2] of The Astrochymist web page[3]. A large portion of these molecules were detected toward Sagittarius (Sgr for short) B2(N). Sgr B2(N) is

part of the Sgr B2 molecular cloud complex, one of the most prominent star-forming regions in our Galaxy and close to its center. There are two major sites of high-mass star formation, Sgr B2(M) and Sgr B2(N), see, for example, Schmiedeke et al. (2016), of which Sgr B2(N) has a greater variety of complex organic molecules (Belloche et al. 2013). It contains two dense compact hot cores, the more prominent Sgr B2(N1), also known as Large Molecule Heimat, and Sgr B2(N2), about 5″ to the north of it (Belloche et al. 2016; Schmiedeke et al. 2016).

Following up on our single-dish survey of the 3 mm wavelength range with the IRAM 30 m telescope (Belloche et al. 2013), we have used the Atacama Large Millimeter/submillimeter Array (ALMA) in its Cycles 0 and 1 to perform a spectral line survey of Sgr B2(N) between 84.1 and 114.4 GHz (Belloche et al. 2016). The name of the survey,

[1] http://www.astro.uni-koeln.de/cdms/molecules
[2] http://www.astrochymist.org/astrochymist_ism.html
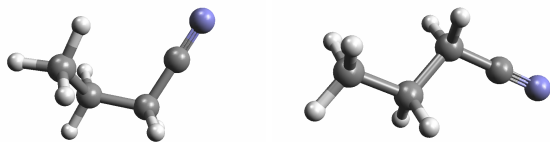[3] http://www.astrochymist.org/

Fig. 1. Schematic depiction of the *gauche* (*left*) and *anti* (*right*) conformers of *normal*-propyl cyanide. The C and N atoms are represented by gray and violet "spheres", respectively, and the H atoms by small, light gray ones.

Exploring Molecular Complexity with ALMA (EMoCA), describes the main motivation of this study. The high angular resolution ($\sim 1.6''$) allows us to separate the emission of the two hot cores, that, in turn, revealed the narrow line width of Sgr B2(N2) (~ 5 km s^{-1}), greatly reducing the line confusion with respect to our previous single-dish survey of Sgr B2(N). As a consequence, we have focused our analysis on Sgr B2(N2) thus far.

The detection of *iso*-propyl cyanide (or *i*-PrCN for short; *i*-C_3H_7CN) as the first branched alkyl molecule in space was one of the first results of EMoCA (Belloche et al. 2014). The laboratory spectroscopic investigation on *i*-PrCN (Müller et al. 2011) was an obvious prerequisite, but the decrease in line confusion was important also because this molecule was not detected in our previous single-dish survey of Sgr B2(N) (Belloche et al. 2013; Müller et al. 2011). Interestingly, *i*-PrCN is not much less abundant than its straight-chain isomer *normal*-propyl cyanide (*n*-PrCN for short; Belloche et al. 2014). Other published results of EMoCA include the detection of the three isotopomers of ethyl cyanide with two ^{13}C (Margulès et al. 2016), an extensive study of deuterated complex organic molecules in Sgr B2(N2) with, for example, the first, albeit tentative, detection of deuterated ethyl cyanide (Belloche et al. 2016), and a study of alkanols and alkanethiols, which yielded a rather stringent upper limit to the column density of ethanethiol in this source (Müller et al. 2016b).

We had detected *n*-PrCN initially in our single-dish study (Belloche et al. 2009). The line intensities of this molecule in our ALMA spectra toward Sgr B2(N2) in combination with its several low-lying vibrational states (Charles et al. 1976; Crowder 1987; Durig et al. 2001) suggested that we should be able to detect transitions of vibrationally excited *n*-PrCN in our ALMA data.

The ground state rotational spectrum has been investigated quite well in the laboratory. Hirota (1962) used microwave spectroscopy between 8 and 32 GHz to study rotational isomerism (i.e., the presence and energetics of different conformers) of *n*-PrCN. He identified two possible conformers, *anti* (*a* for short, also known as *trans*) with a dihedral CCCC angle of 180° and *gauche* (*g* for short, also known as *synclinal*) with a dihedral CCCC angle of about ±60°, see also Fig. 1. The two *gauche* conformers are indistinguishable. Demaison & Dreizler (1982) studied the ^{14}N quadrupole structure of the *anti* conformer by Fourier transform microwave spectroscopy. Vormann & Dreizler (1988) used the same technique between 4.8 and 26.4 GHz for an extensive study of the rotational spectrum, quadrupole structure, and methyl internal rotation of both conformers. Wlodarczak et al. (1988) extended the measurements into the millimeter region, measured the dipole moment components, and determined from intensity measurements that the *anti* conformer is lower in energy than *gauche* by 1.1 ± 0.3 kJ mol^{-1} (or 92 ± 25 cm^{-1} or 132 ± 36 K), in line with the estimate by Hirota (1962) that the energy difference between the two is

small, perhaps less than 1 kcal mol^{-1} (or 350 cm^{-1} or 504 K). However, Charles et al. (1976) and Traetteberg et al. (2000) determined from earlier infrared (IR) spectroscopy of solid, liquid, and gaseous samples and from electron diffraction of a gaseous sample that the *gauche* conformer is lower in energy. Durig et al. (2001) used IR spectroscopy of *n*-PrCN dissolved in liquid Xenon (−60 to −100 °C) to determine that the *gauche* conformer is lower than *anti* by 0.48 ± 0.04 kJ mol^{-1} (or 40 ± 3 cm^{-1} or 58 ± 4 K). Using our ALMA data, we modeled the *anti/gauche* energy difference and found it to be fully consistent with the latter value (Belloche et al. 2014).

The experimental data on excited vibrational states were rather limited. Hirota (1962) also observed vibrational satellites of *n*-PrCN in his microwave study and published rotational constants for the four lowest states of each conformer. They belong in either case to the three lowest fundamental states as well as to the overtone state of the lowest one. These parameters turned out to be sufficient for assignments of laboratory spectra near 1 cm wavelength, but were by far too imprecise for assignments in our ALMA data.

Therefore, we recorded rotational spectra of *n*-PrCN in two spectral windows, 36 to 70 GHz and 89 to 127 GHz, and analyzed the four lowest vibrational states of each conformer. These results enabled us to detect transitions of all four states in our ALMA data. Details on our laboratory spectroscopic investigations are given in Sect. 2. Background information on the rotational and vibrational spectroscopy of *n*-PrCN is provided in Sect. 3. Results of our current laboratory spectroscopic study and a related discussion are given in Sect. 4. Section 5 describes the analyses of our ALMA data, and Sect. 6 contains conclusions and an outlook.

2. Laboratory spectroscopic details

All measurements were carried out at room temperature at the Universität zu Köln in two connected 7 m long double path absorption cells with inner diameter of 100 mm which were equipped with Teflon windows. A commercial sample of *n*-PrCN was flowed slowly through the cell at pressures of around 1 Pa. We used frequency modulation throughout with demodulation at $2f$, which causes an isolated line to appear approximately as a second derivative of a Gaussian.

The entire region between 36 and 70 GHz was covered in successive scans with an Agilent E8257D microwave synthesizer as source and a Schottky diode detector. The point spacing was 20 kHz, and at each point, data were accumulated for 20 ms. One upward scan and one downward scan were coadded after completion of the spectral recording. Later, we recorded smaller sections of 2 to 6 MHz widths around the predicted positions of *b*-type transition of the *anti* conformer employing much longer overall integration times which reached up to 50 min for 6 MHz. The entire region between 89.25 and 126.75 GHz was covered similarly using a Virginia Diode, Inc. (VDI) tripler driven by a Rohde & Schwarz SMF 100A synthesizer as source and a Schottky diode detector. The point spacing in this frequency region was 60 kHz, and the integration time per point was again 20 ms with scans in both directions Further details on the spectrometer system are available elsewhere (Bossa et al. 2014; Walters et al. 2015).

Despite the long integration times, the confusion limit was not reached by far in either of these two large spectral windows. The sensitivity of the spectrometer systems varied greatly with frequency. It was very low at the lower ends of both frequency windows and near 127 GHz. In addition, there were sections in

which the sensitivity was very low within the spectral windows. In addition, intensities sometimes changed drastically within a few megahertz. Nevertheless, relative intensities could be used frequently as guidance for assignments over several tens to a few hundreds of megahertz with only modest adjustments, in particular to check for possible blending.

3. Spectroscopic properties of *n*-propyl cyanide

The molecule *n*-propyl cyanide, also known as butyronitrile or 1-cyanopropane, exists in two distinguishable conformers, *gauche* and *anti*, with the former being doubly degenerate with respect to the latter. Durig et al. (2001) showed that *gauche* is lower in energy than *anti* by 40 ± 3 cm^{-1}.

The *anti* conformer is an asymmetric rotor with $\kappa = (2B - A - C)/(A - C) = -0.9893$ close to the prolate limit of -1. Successive R-branch transitions are approximately spaced by $B + C \approx 4.4$ GHz. The A rotational constant, ~ 24 GHz, is a measure for the K_a level spacing as the $K_a = J$ levels are roughly given by $A K_a^2$. The *gauche* conformer is more asymmetric ($\kappa = -0.8471$) with a wider spacing between consecutive R-branch transitions ($B + C \approx 6.0$ GHz) and a narrower K_a level spacing ($A \approx 10.1$ GHz).

The large dipole moment is caused predominantly by the CN group. Wlodarczak et al. (1988) determined the *a-n*-PrCN dipole moment components as $\mu_a = 3.597 \pm 0.059$ D and $\mu_b = 0.984 \pm 0.015$ D; $\mu_c = 0$ by symmetry. Müller et al. (2011) presented quantum chemical calculations on properties of *i*-PrCN, *a-n*-PrCN, and *cyclo*-PrCN from which Belloche et al. (2014) concluded that μ_a is likely underestimated by about 10%. They proposed $\mu_a = 4.0$ D and suggested that the underestimation of μ_a could be responsible, at least in part, for the incorrect energy ordering of the conformers by Wlodarczak et al. (1988). The results for *g-n*-PrCN were $\mu_a = 3.272 \pm 0.037$ D and $\mu_b = 2.139 \pm 0.030$ D under the assumption of $\mu_c = 0$ (Wlodarczak et al. 1988). Quantum chemical calculations yield $\mu_c \approx 0.45$ D (Durig et al. 2001), in line with the value mentioned by Belloche et al. (2014).

The orientation of the ^{14}N quadrupole tensor in a CN group is usually very close to this bond. This leads to $\chi_{aa} = -3.44$ MHz and $\chi_{cc} = 2.06$ MHz for *a-n*-PrCN and $\chi_{aa} = -1.68$ MHz and $\chi_{cc} = 1.94$ MHz for *g-n*-PrCN (Vormann & Dreizler 1988); χ_{bb} is determined from the tracelessness of the tensor.

The *n*-PrCN molecule has 12 atoms, its vibrational spectrum consists of $3 \times 12 - 6 = 30$ fundamental vibrations. The *gauche* conformer has C_1 symmetry, so all vibrations belong to the symmetry class *a*. In contrast, the *anti* conformer has C_S symmetry, and 18 vibrations belong to the symmetry class *a'* and 12 to the symmetry class *a''* (Crowder 1987). Durig et al. (2001) presented the most comprehensive study on the vibrational spectroscopy of this molecule. They measured the gas phase IR spectrum in the mid-IR (down to 300 cm^{-1}), and the solid-state IR and the liquid-state Raman spectra covered all fundamental vibrations. They supplemented these data by quantum chemical calculations at the MP2/6−31G* level; in addition, they presented scaled values for the fundamental vibrations to account for anharmonicity and model deficiencies. Figure 2 displays the vibrational states below 400 cm^{-1}.

In order to evaluate contributions of vibrational states to the partition function Q of *n*-PrCN, we calculated vibrational correction factors F_{vib} to the rotational partition function values Q_{rot} ($Q = F_{vib} \times Q_{rot}$) at the seven CDMS standard temperatures plus two additional ones (120 K and 180 K). Scaled values from a quantum chemical calculation (Durig et al. 2001) were taken
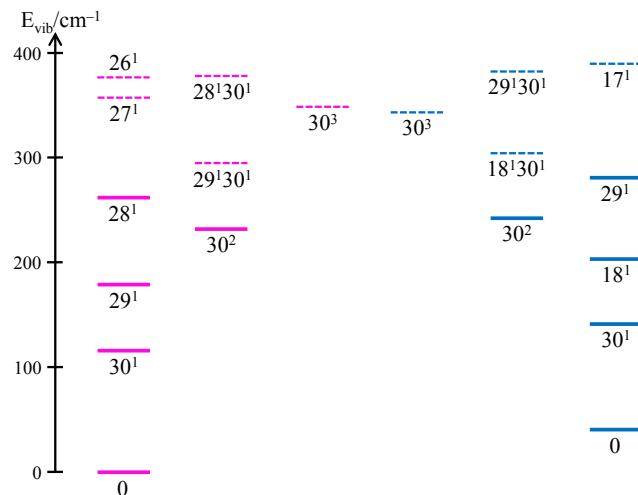

Fig. 2. Vibrational states of *normal*-propyl cyanide up to vibrational energies of 400 cm^{-1}. The *gauche* states are shown on the *left-hand side*, those of *anti* on the *right-hand side*. The ground vibrational states and the four vibrational states each of the present study are indicated by solid, thick lines, additional states by dashed, thin lines.

Table 1. Rotational partition function Q_{rot} and vibrational correction factors F_{vib} to the rotational partition function values of *n*-propyl cyanide at selected temperatures T.

T (K)	Q_{rot}	F_{vib}
300.0	254 102.1111	9.9477
225.0	162 159.7064	4.4642
180.0	114 139.6161	2.8253
150.0	85 494.8293	2.1160
120.0	59 864.2360	1.6192
75.0	27 985.6804	1.1684
37.5	8997.8511	1.0129
18.75	2968.9170	1.0001
9.375	1032.0718	1.0000

for vibrational energies of the lowest three fundamental modes of the *gauche* conformer and the gas phase experimental values from the same work for all others. Contributions of overtone and combination states were evaluated in the harmonic approximation. The resulting values of Q_{rot} and F_{vib} are given in Table 1.

Uncertainties in the vibrational energies, neglect of differences in the vibrational energies between the two conformers and the neglect of anharmonicity contribute to errors in F_{vib}. We estimate these errors to be a few percent of $F_{vib} - 1$ at low temperatures and possibly many tens of percent at 300 K.

A plethora of low-lying vibrational states of *n*-PrCN are populated at room temperature such that only about one tenth of the molecules are in the ground vibrational states of the *gauche* or *anti* conformer. The lowest vibrational state ($v_{30} = 1$ for both conformers) has predominantly the character of a torsion around the central C atoms (Charles et al. 1976; Crowder 1987; Durig et al. 2001) and could be called ethyl torsion. The next lowest state ($v_{29} = 1$ or $v_{18} = 1$ for *gauche* and *anti*, respectively) is a mixed bending vibration involving mostly the CCN angle and the CCC angle with the cyano-C. The next vibrational state is $v_{30} = 2$, followed by $v_{28} = 1$ (*gauche*) or $v_{29} = 1$ (*anti*) with

predominantly methyl torsional character (Charles et al. 1976; Crowder 1987; Durig et al. 2001).

4. Spectroscopic results and their discussion

We used Pickett's SPCAT and SPFIT programs (Pickett 1991) to predict and fit rotational spectra of vibrationally excited n-PrCN. Vibrational changes ΔX of a spectroscopic parameter X are usually considerably smaller in magnitude than the magnitude of X. Using ground state spectroscopic parameters and fitting the vibrational changes has two distinct advantages. First, the ground state parameters usually account for a substantial fraction of the excited state parameters. Second, the number of spectroscopic parameters used in the fit is considerably smaller than using independent sets of parameters for each state. Earlier examples include excited states of bromine dioxide (Müller et al. 1997a), chlorine dioxide (Müller et al. 1997b), and the main and minor isotopologs of methyl cyanide (Müller et al. 2015, 2016a). We defined $\Delta X = X_{v=1} - X_0$ and $\Delta\Delta X = X_{v=2} - X_0 - 2\Delta X$. The ground state rotational and centrifugal distortion parameters of n-PrCN were taken from Belloche et al. (2009), who combined data from earlier publications (Demaison & Dreizler 1982; Vormann & Dreizler 1988; Wlodarczak et al. 1988, 1991), and were kept fixed in the present analyses. Calculated values for ΔA, ΔB, and ΔC of each vibrational state of both conformers were derived from Hirota (1962).

We recognized fairly early that a considerable fraction of the transitions in the laboratory spectrum, usually weaker ones, displayed partially resolved ^{14}N hyperfine structure (HFS) splitting caused by the nuclear quadrupole moment of ^{14}N, as is shown in Fig. 3. Therefore, we generated predictions of the rotational spectra of excited states of n-PrCN with and without considering HFS and compared the spectral recordings with the results of both predictions. The HFS parameters were taken from Vormann & Dreizler (1988) and kept fixed in the fits.

The spin of the ^{14}N nucleus ($I = 1$) leads to three HFS levels. Except for the lowest J quanta, this leads to three stronger HFS components with $\Delta F = \Delta J$ and $F = J, J \pm 1$. The $F = J \pm 1$ components are almost always blended in our spectra such that a relatively well-resolved HFS pattern has an intensity ratio of nearly 2:1 (see Fig. 3). If the $F = J$ component is close to the $F = J \pm 1$ line, it appears weaker. This component was then given a larger uncertainty or it was not used in the fit if its position appeared to be affected too much by the proximity of the stronger $F = J \pm 1$ line. The $F = J \pm 1$ line could also appear weaker than expected if the two components were separated by several tens of kilohertz.

4.1. The gauche conformer

The gauche conformer has sizable a- and b-dipole moment components which facilitate assignments of corresponding transitions. Moreover, a-type transitions alone lead to fairly accurate values of A, D_K, etc. because the conformer is quite far away from the prolate symmetric limit. The asymmetry leads to a rapid increase of the asymmetry splitting for a given K_a with increasing J, or, in other words, to resolved asymmetry splitting at relatively low values of J. In addition, transitions with $K_c = J''$ are almost degenerate (or oblate paired) close to 127 GHz.

We searched initially for a-type R-branch transitions ($\Delta J = +1$) with $K_a \le 2$ starting at low frequencies. These transitions were found easily close to the predicted frequencies. After refinement of the spectroscopic parameters, assignments were extended to higher K_a values and to the 89−127 GHz frequency window. Once the assignments reached $K_a = 5$ we assigned b-type R-branch transitions with $K_a = 1 \leftrightarrow 0$ and then $K_a = 2 \leftrightarrow 1$. These transitions were mostly found easily and close to the predictions. Assignments of transitions pertaining to the $v_{28} = 1$ state were not as straightforward, as will be discussed in greater detail below.

The a-type R-branch transitions displayed partially resolved ^{14}N HFS structure for the two highest values of K_a ($J'' - 1$ and J'') in the 36−70 GHz window, as can be seen in the upper trace of Fig. 3. The b-type transitions are also affected significantly by HFS splitting in certain quantum number ranges, especially Q-branch transitions ($\Delta J = 0$) with low values of K_a, see lower trace of Fig. 3, as well as some a-type Q-branch transitions with $\Delta K_a = 0$ and 2.

4.1.1. $v_{30} = 1$ and 2

The quantum chemically calculated vibrational energy of $v_{30} = 1$ is 116 cm^{-1} both scaled and unscaled (Durig et al. 2001). A shoulder in the Raman spectrum of the liquid sample at 114 cm^{-1} agrees well with the calculated value, whereas the position of a strong feature in the solid-state IR spectrum at 140 cm^{-1} agrees less well (Durig et al. 2001). The calculated energy of $v_{30} = 2$ in the harmonic approximations is 232 cm^{-1}. Anharmonicity is probably small; we will discuss this aspect in the context of $v_{30} = 2$ of the *anti* conformer and its interaction with $v_{18} = 1$ in Sect. 4.2.3.

Figure 3 shows not only the partial HFS splitting, but also the decrease in intensity upon excitation of v_{30}. The a-type R-branch transitions reach $J = 23-22$ for $K_c = J$ near 127 GHz and $J = 21-20$ for $K_a \ge 3$. We assigned transitions up to $K_a = 20$ for both $v_{30} = 1$ and 2. Q-branch transitions with $\Delta K_a = 0$ or 2 are considerably weaker. Assignments with $\Delta K_a = 0$ reach $K_a = 11$ and $J = 61$ for $v_{30} = 1$ and $K_a = 8$ and $J = 45$ for $v_{30} = 2$. In the case of $\Delta K_a = 2$ we assign up to $K_a = 8-6$ and $J = 43$ for $v_{30} = 1$ and up to $K_a = 6-4$ and $J = 34$ for $v_{30} = 2$. The b-type transitions involve ^rR, ^pR, and ^rQ transitions up to $K_a = 11$ for both states and $J = 65$ and 63 for $v_{30} = 1$ and 2, respectively. The superscripts indicate $\Delta K_a = +1$ (r) and -1 (p), respectively. There was evidence for b-type transitions with even higher K_a in the spectral recordings, but because of their weakness and greater sparseness we refrained from including them in the line lists at present. We point out that identification of $v_{30} = 2$ transitions was greatly facilitated, especially for very weak transitions, by $v_{30} = 1$ assignments already included in the fit because the ground state spectroscopic parameters and the $v_{30} = 1$ vibrational corrections (multiplied by two) accounted quite well for the $v_{30} = 2$ transition frequencies.

The vibrational changes of the parameters for $v_{30} = 1$ and the second changes for $v_{30} = 2$ are given in Table 2 together with ground state parameters and vibrational changes for $v_{29} = 1$ and $v_{28} = 1$. We determined a full set of vibrational changes up to fourth order along with several sixth order changes; the set of second changes is somewhat smaller, as can be expected. The quadrupole splitting showed systematic changes from $v_{30} = 0$ to 2 which permitted determination of a vibrational change to χ_{aa}.

4.1.2. $v_{29} = 1$

Durig et al. (2001) give 163 cm^{-1} as scaled calculated value, and the unscaled value is 1 cm^{-1} higher. Their liquid- and solid-state Raman spectra display a medium strong band at 180 cm^{-1}, in moderate agreement. If we assume that results of quantum
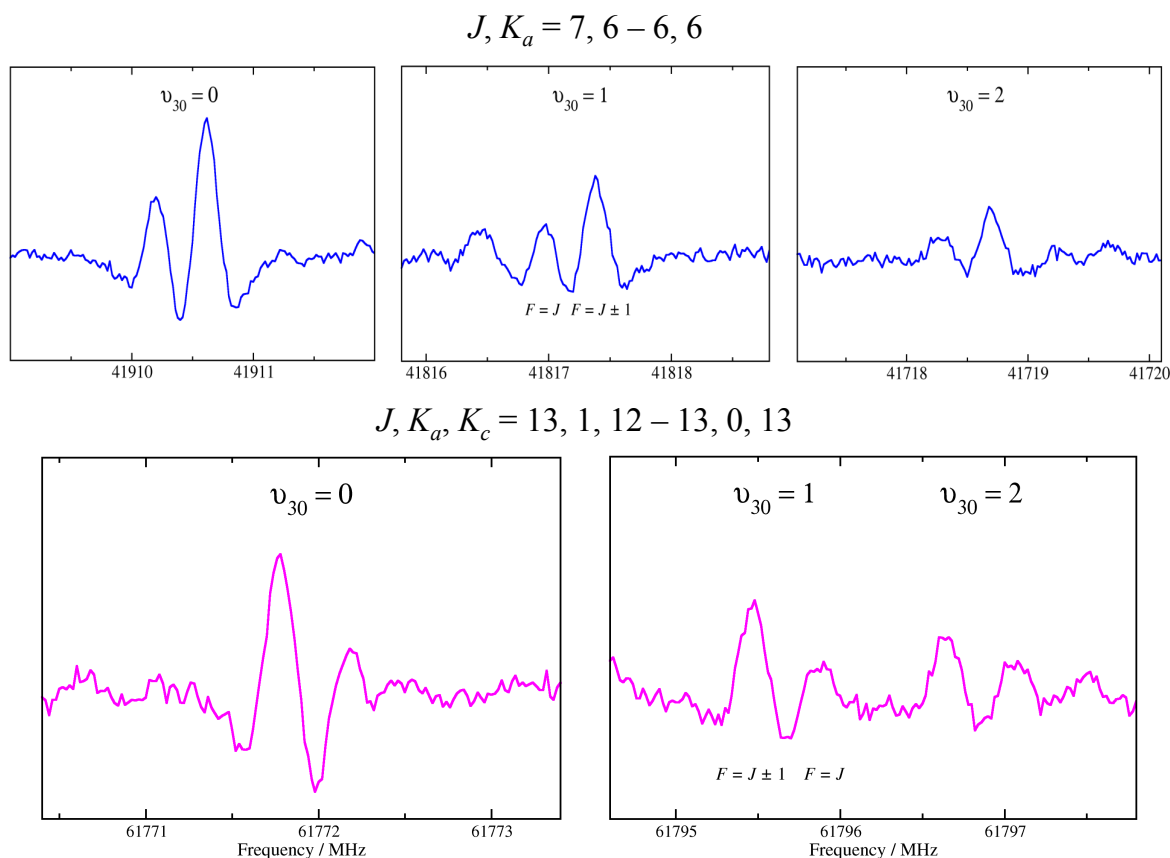
Fig. 3. Sections of the rotational spectrum of *g-n*-PrCN showing transitions with partially resolved ^{14}N quadrupole splitting. The upper trace shows the 7, 6−6, 6 *a*-type *R*-branch transition with a 1:2 HFS pattern, the lower trace shows the 13, 1, 12−13, 0, 13 *b*-type *Q*-branch transition with a 2:1 HFS pattern. Transitions for $v_{30} = 0$, 1, and 2 are shown from *left to right* in both cases; the vibrational labels are given above the two HFS components, their assignments are indicated below the $v_{30} = 1$ lines.

chemical calculations are similar in quality with respect to the values of the free, gaseous molecule of both conformers and that this also holds for the results from liquid- and solid-state Raman spectra, then our experimentally determined energy difference between $v_{30} = 2$ and $v_{18} = 1$ (see Sect. 4.2.3) provides evidence that the vibrational energy of $v_{29} = 1$ of gaseous *g-n*-PrCN is closer to 163 cm^{-1} than to 180 cm^{-1}.

The assignments of *a*-type *R*-branch transitions and of *b*-type transitions took place in a similar way as for $v_{30} = 1$ and 2. Assignment of weaker lines was often more difficult than in the case of $v_{30} = 2$ because larger uncertainties made unambiguous assignments more difficult even though corresponding $v_{30} = 2$ lines were slightly weaker; predictions of $v_{30} = 2$ frequencies were better because of the $v_{30} = 1$ assignments, see also Sect. 4.1.1. Fewer *b*-type transitions extending not as high in *J* are probably the most important reason why we have not been able to assign weak *a*-type *Q*-branch transitions in $v_{29} = 1$.

Excluding $\Delta\chi_{aa}$, the number of spectroscopic parameters in the fit of $v_{29} = 1$ is the same as that for $v_{30} = 1$, but the choice of sixth order parameters is different, see Table 2.

4.1.3. $v_{28} = 1$

The CH$_3$ torsional mode is expected to be quite anharmonic. The unscaled vibrational energy for this mode is 276 cm^{-1}, and the scaled one 262 cm^{-1} (Durig et al. 2001). These authors assigned a weak band at 265 cm^{-1} in the IR spectrum of a solid sample,

and also a very weak feature at 244 cm^{-1} in the Raman spectrum of the liquid. We note, however, that the agreement of the latter vibrational energy agrees better with their scaled value for the corresponding mode of the *anti* conformer, see also Sect. 4.2.2.

Assignments of *a*-type *R*-branch transitions with $K_a \leq 2$ were straightforward also for $v_{28} = 1$. Absorption features of higher K_a transitions, however, often appeared somewhat weaker and broader than predicted and/or showed a weaker shoulder; some transitions even appeared split into two. We suspect that these features are caused by methyl internal rotation as $v_{28} = 1$ should possess considerable methyl torsion character (Charles et al. 1976; Crowder 1987; Durig et al. 2001; Castro et al. 2011). The measured line center usually agreed sufficiently well with the calculated positions; however, in the case of a line that was split into two, the average position did not always agree well enough with the calculated position and was weighted out.

We were able to assign several *b*-type *R*-branch transitions with $K_a = 1 \leftrightarrow 0$ and $2 \leftrightarrow 1$. However, some of the lower *J* transitions or *Q*-branch transitions with the same K_a values were quite weak and appeared somewhat displaced from their predicted positions. Their frequencies could not be reproduced with one set of reasonable spectroscopic parameters. Assignment of *b*-type transitions with higher K_a proved to be difficult; most promisingly, we made tentative assignments of several $K_a = 5-4$ *R*-branch transitions. However, it was difficult to fit these transitions together with the previous assignments. In addition, it was not possible to make any further unambiguous assignments.

Table 2. Spectroscopic parameters X (MHz) of *gauche-n*-propyl cyanide and first (ΔX) and second ($\Delta\Delta X$) changes of low-lying vibrational states.

Parameter	$v = 0$ X	$v_{30} = 1$ ΔX	$v_{30} = 2$ $\Delta\Delta X$	$v_{29} = 1$ ΔX	$v_{28} = 1$ ΔX
A	10 060.416 5(11)	58.641 9(3)	3.732 3(5)	23.723 7(5)	−36.927 9(135)
B	3267.662 41(30)	−7.938 29(5)	−0.603 51(11)	2.493 94(13)	2.252 06(85)
C	2705.459 57(29)	−5.173 90(5)	−0.159 73(11)	0.431 86(12)	−0.175 62(44)
$D_K \times 10^3$	60.235(6)	5.005(4)	0.782(5)	−0.829(4)	−2.2[a]
$D_{JK} \times 10^3$	−18.264 7(12)	−0.656 7(3)	−0.138 5(3)	0.155 7(8)	0.335 9(23)
$D_J \times 10^6$	3195.06(21)	7.76(4)	6.36(8)	−20.64(22)	8.94(57)
$d_1 \times 10^6$	−1037.470(55)	−8.029(10)	−2.455(22)	1.804(33)	−5.61(49)
$d_2 \times 10^6$	−77.186(18)	−3.605(3)	−0.280(7)	−1.244(18)	−1.19(27)
$H_K \times 10^6$	1.806(18)	0.476(21)			
$H_{KJ} \times 10^6$	−0.517 3(35)	−0.109 5(10)		−0.042 8(41)	
$H_{JK} \times 10^9$	9.92(68)	5.52(8)		−6.26(27)	
$H_J \times 10^9$	4.486(56)			−0.524(95)	
$h_1 \times 10^9$	2.505(29)	−0.148(3)	−0.159(5)		
$h_2 \times 10^{12}$	525.(14)			180.(15)	
$h_3 \times 10^{12}$	111.3(31)	5.0(5)		48.1(64)	
$L_{KKJ} \times 10^{12}$	30.6(31)				
$L_{JK} \times 10^{12}$	−4.11(78)				
χ_{aa}	−1.683(4)	−0.061(10)			
χ_{bb}	−0.252(5)[b]				
χ_{cc}	1.935(5)[b]				

Notes. Watson's S reduction has been used in the representation I^r. Ground state parameters are from Belloche et al. (2009) except quadrupole parameters which are from Vormann & Dreizler (1988). Numbers in parentheses are one standard deviation in units of the least significant figures. Parameters without uncertainties were estimated and kept fixed in the analyses. $\Delta X = X_{v=1} - X_0$; $\Delta\Delta X = X_{v=2} - X_0 - 2\Delta X$. [a] Estimated value, see Sect. 4.1.3. [b] Derived values.

The set of spectroscopic parameters for $v_{28} = 1$ is smaller than those for the other vibrational states of *g-n*-PrCN. We estimated $\Delta D_K = -2.2$ kHz to accommodate the fairly secure assignments of *b*-type transitions with $K_a \leq 2$.

4.2. The anti conformer

The *anti* conformer is much closer to the prolate symmetric top limit than *gauche*, which makes the determination of A, D_K, etc. difficult from *a*-type transitions alone. The smaller magnitude of the *b*-dipole moment component of this conformer and its larger A rotational constant make it more difficult to assign *b*-type transitions. Its much smaller asymmetry leads to unresolved asymmetry splitting for $K_a = 4$ at low frequencies and also throughout the two frequency windows for $K_a > 4$. Furthermore, most transitions ($K_a \geq 3$) of a given vibrational state occur in a narrow frequency range in the two frequency windows, as shown in Fig. 4, which often leads to blending of lines.

Initial assignments focused on $K_a \leq 2$ *a*-type *R*-branch transitions at lower frequencies, as in the case of the *gauche* conformer. Assignments were extended to higher frequencies and to higher K_a transitions with refined predictions. Overlap of transitions with different values of K_a made the assignments less straightforward in the early stages than for the *gauche* conformer.

Splitting caused by the ^{14}N quadrupole coupling affects a much larger fraction of the *a*-type *R*-branch transitions of the *anti* conformer because the quadrupole coupling parameters are much larger in magnitude than for the *gauche* conformer, most importantly χ_{aa}. The *a*-type *Q*- or *P*-branch transitions of the *anti* conformer were too weak to be identified.

Subsequently, we attempted to assign *b*-type transitions with $K_a = 1 \leftrightarrow 0$. These transitions were too weak in our spectral recordings covering 36 to 70 GHz, but sufficiently strong in the 89 to 127 GHz region. However, the density of lines at these low intensity levels together with the relatively large uncertainties made unambiguous assignments difficult. Therefore, we recorded smaller sections around the positions of the *b*-type transitions in the 36−70 GHz region with much longer integration time. In these recordings, we detected several candidate lines for each vibrational state. Further details will be provided below.

4.2.1. $v_{30} = 1$

The calculated scaled and unscaled vibrational energy of $v_{30} = 1$ is 101 cm^{-1}; this compares well with a strong band in the solid-state Raman spectrum at 99 cm^{-1} (Durig et al. 2001).

The *a*-type transitions have $J = 9−8$ at low frequencies and $J = 28−27$ at high frequencies; in the case of $K_a = 1$, the $29_{1,29}−28_{1,28}$ transition falls into the frequency ranges we have covered and analyzed thus far. The K_a quantum numbers extend to 24, almost reaching the theoretical limit of 27 ($K_{a,\max} \leq J_{\max}$). We were able to identify 10 *b*-type transitions in the smaller spectral recordings below 70 GHz, the lowest frequency assignment was near 53 GHz. We assigned 14 additional *b*-type transitions between 89 and 127 GHz. The transitions are spread quite evenly among $^rR_0$, $^pR_1$, and $^rQ_0$ transitions; the subscript indicates K_a in the lower energy rotational level, and the J range covers 8 to 48.
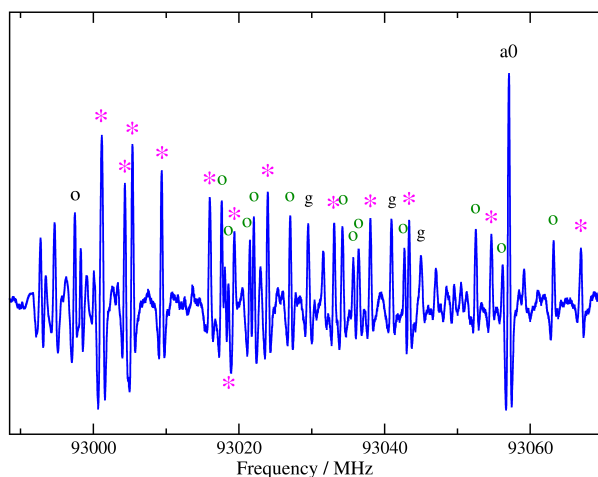
Fig. 4. Section of the rotational spectrum of *n*-PrCN displaying the clustering of *a*-type *R*-branch transitions of the *anti* conformer with higher values of K_a. Magenta asterisks indicate transitions of $v_{30} = 1$, green circles those of $v_{18} = 1$, a black circle a transition of $v_{30} = 2$, "a0" labels a ground state transition, and a "g" labels transitions of the gauche conformer.

We fit $v_{30} = 1$ and 2 together from the beginning. It required a modest set of vibrational changes to reproduce the $v_{30} = 1$ transitions well. These are changes to the rotational and quartic centrifugal distortion parameters and to H_{KJ}. We measured accurate frequencies of both $\Delta F = J \pm 1$ as well as $\Delta F = J$ for several transitions with higher K_a of $v_{30} = 1$ and to a lesser extent for $v_{30} = 2$. In a trial fit, we obtained $\Delta \chi_{aa} = 10 \pm 35$ kHz which was omitted from the final fit. The resulting spectroscopic parameters are given in Table 3 together with parameters of other vibrational states of the anti conformer.

Many of the vibrational changes ΔX are much smaller than the ground state parameters X themselves, as is usually expected. The magnitude of ΔA, however, is relatively large with respect to ΔB and ΔC, even if we take into account that A is about one order of magnitude larger than either B or C. The ΔA value of $v_{18} = 1$ is of similar magnitude and of opposite sign, suggesting the large magnitudes are caused to a considerable amount by the non-resonant Coriolis interaction between these states. Strong, albeit resonant, Coriolis interaction was identified between the corresponding modes $v_{13} = 1$ and $v_{21} = 1$ of the lighter homolog ethyl cyanide (Laurie 1959). We have carried out trial fits that have shown that $|\zeta_a| \approx 0.82$ yields $\Delta A \approx -37$ MHz for both states and affects several of the vibrational changes of the distortion parameters considerably. Accurate harmonic force field calculations would be required to establish the actual value of $|\zeta_a|$ as well as the non-zero value of $|\zeta_b|$. Such calculations are beyond the aim of the current study.

4.2.2. $v_{29} = 1$

Durig et al. (2001) calculated an unscaled value of 254 cm^{-1} for the vibrational energy of the CH$_3$ torsional mode and a scaled value of 241 cm^{-1}. They do not assign any experimental feature to this mode. We point out that a very weak band in the Raman spectrum of the liquid sample at 244 cm^{-1} agrees well with the scaled value; Durig et al. (2001) assigned this band to the CH$_3$ torsional mode of the gauche conformer, see also Sect. 4.1.3.

The assignments of *a*-type transitions pertaining to $v_{29} = 1$ proceeded analogously to those of $v_{30} = 1$, but extended only to $K_a = 18$ mainly because it is the highest of the vibrational

states of *n*-PrCN in the present study. As can be seen in Fig. 4, not only do high-K_a transitions of each vibrational state of *a*-*n*-PrCN occur in a narrow frequency region, but also those of other vibrational states are often very close. Therefore, blending of lines reduced the number of assignments. For example only $J = 28-27$ could be seen as apparently not blended in the case of $K_a = 17$. Even though there are two vibrational states of *a*-*n*-PrCN close to this state, $v_{18} = v_{30} = 1$ and $v_{30} = 2$, we did not find clear evidence for perturbations of $v_{29} = 1$.

We found six lines with approximately the right intensity close to the predicted frequencies of $K_a = 1 \leftrightarrow 0$ *b*-type transitions in the long integration, narrow spectral recordings between 54 and 67 GHz. These lines could be fit within experimental uncertainties on average. With improved predictions, six more transitions close to the predicted positions were tentatively assigned in the 89 to 127 GHz region. The twelve *b*-type transitions, however, could not be fit within experimental uncertainties with a reasonable set of spectroscopic parameters. It is possible that some positions are affected by unrecognized blending. Even though $v_{29} = 1$ should have predominantly methyl torsion character, we did not find any clear evidence for broadening or even splitting of lines due to torsion. Nevertheless, we do not rule out that the unsatisfactory fitting of the *b*-type transitions may be related to torsional effects. We have omitted the lines from the final line list because of this unclear situation.

The set of spectroscopic parameters in Table 3 is much smaller for $v_{29} = 1$ than it is for $v_{30} = 1$; only changes for the rotational parameters, D_{JK}, D_J, and H_{KJ} were needed to fit the *a*-type transitions of $v_{29} = 1$ satisfactorily.

4.2.3. $v_{18} = 1$ and $v_{30} = 2$

Whereas Durig et al. (2001) measured a medium strong band in the Raman spectrum of liquid and solid samples at 180 cm^{-1}, they report a scaled calculated value of 163 cm^{-1}; the unscaled value is 1 cm^{-1} higher. The calculated vibrational energy of $v_{30} = 2$ is 202 cm^{-1} in the harmonic approximation.

The initial assignments of $v_{30} = 2$ and $v_{18} = 1$ *a*-type transitions proceeded in a similar way to those of $v_{30} = 1$ and $v_{29} = 1$. However, fitting transitions of $v_{30} = 2$ with $K_a = 10$ and 11 required a value of $\Delta\Delta H_{KJ}$ that was larger than ΔH_{KJ} of $v_{30} = 1$. Furthermore, this parameter was not sufficient to reproduce transitions having $K_a = 12$ and 13, and transitions with even higher K_a could not be assigned with confidence. Weighting out all lines with $K_a \geq 10$ and constraining $\Delta\Delta H_{KJ}$ such that its ratio with ΔH_{KJ} is equal to the $\Delta\Delta D_{JK}$ to ΔD_{JK} ratio showed that the $K_a = 13$ transitions had residuals between 1.56 and 2.95 MHz for $20 \leq J'' \leq 27$. These residuals were almost perfectly matched by residuals between -1.65 and -2.95 MHz in $K_a = 14$ of $v_{18} = 1$, indicative of a $\Delta K_a = \pm 1$ rotational (also known as Coriolis-type) resonance between these states. Figure 5 displays the K_a level structure of these states with the resonant interactions highlighted. We estimated the energy difference $E(30^2-18)$ between the two states and adjusted the first order Coriolis parameter G_c. After both parameters were fit and updated, predictions were generated, and we were able to assign transitions with higher K_a for both states. However, they soon showed deviations rapidly increasing with K_a in opposite directions for the two vibrations, indicative of a Fermi resonance. After inclusion of a Fermi parameter F in the fit, assignments could be extended up to $K_a = 20$. Transitions with even higher K_a were too weak to be assigned with confidence.

We found ten $K_a = 1 \leftrightarrow 0$ *b*-type transitions in the long integration, narrow spectral recordings between 38 and 70 GHz

Table 3. Spectroscopic parameters X (MHz) of *anti-n*-propyl cyanide and first (ΔX) and second ($\Delta\Delta X$) changes of low-lying vibrational states and parameters describing the interaction between $v_{18} = 1$ and $v_{30} = 2$.

Parameter	$v = 0$ X	$v_{30} = 1$ ΔX	$v_{30} = 2$ $\Delta\Delta X$	$v_{18} = 1$ ΔX	$v_{29} = 1$ ΔX
A	23 668.319 3(14)	−810.855(12)	93.495(77)	738.035(75)	−0.702(137)
B	2268.146 89(15)	1.451 97(7)	0.163 73(12)	5.158 11(20)	−2.318 97(14)
C	2152.963 95(17)	5.005 71(6)	0.158 67(29)	1.975 84(33)	−1.495 34(14)
$D_K \times 10^3$	240.65(3)	−263.6(80)			
$D_{JK} \times 10^3$	−10.826 3(9)	0.496 8(5)	0.138 0(12)	−0.354 6(11)	0.092 4(9)
$D_J \times 10^6$	398.67(7)	7.94(3)		−1.80(8)	−0.45(6)
$d_1 \times 10^6$	−46.64(4)	1.45(3)		−1.14(9)	
$d_2 \times 10^6$	−0.590(6)	2.416(24)		−1.760(52)	
$H_K \times 10^6$	2.5				
$H_{KJ} \times 10^9$	372.4(24)	63.5(14)	17.[a]		63.1(39)
$H_{JK} \times 10^9$	−20.67(20)				
$H_J \times 10^9$	0.353(11)				
$h_1 \times 10^9$	0.117(14)				
χ_{aa}	−3.440(4)				
χ_{bb}	1.385(5)[b]				
χ_{cc}	2.055(5)[b]				
Interaction $v_{18} = 1/v_{30} = 2$					
$E(30^2 - 18) \times 10^{-3}$			1017.98(61)		
$F(18, 30^2) \times 10^{-3}$			36.48(44)		
$G_c(18, 30^2)$			129.32(16)		

Notes. Watson's S reduction has been used in the representation I^r. Ground state parameters are from Belloche et al. (2009) except quadrupole parameters which are from Vormann & Dreizler (1988). Numbers in parentheses are one standard deviation in units of the least significant figures. Parameters without uncertainties were estimated and kept fixed in the analyses. $\Delta X = X_{v=1} - X_0$; $\Delta\Delta X = X_{v=2} - X_0 - 2\Delta X$. [a] Estimated value, see Sect. 4.2.3. [b] Derived values.
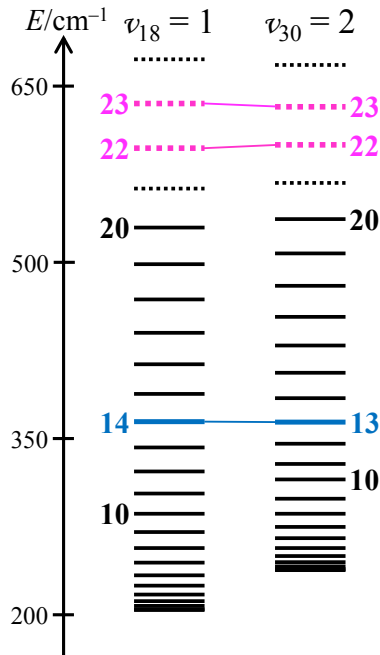
Fig. 5. K_a level structure of $v_{18} = 1$ and $v_{30} = 2$ of *a-n*-PrCN displaying the $\Delta K_a = 1$ rotational (Coriolis-type) resonance as well as the $\Delta K_a = 0$ Fermi resonance. The most strongly interacting levels are shown with colored lines and are connected by thin lines. Dashed lines indicate K_a levels not accessed in the present study.

for $v_{18} = 1$ and seven between 54 and 67 GHz for $v_{30} = 2$; nine and seven more, respectively, were found between 89 and 127 GHz. The J range covers 13−30 and 8−31 for $v_{18} = 1$ and $v_{30} = 2$, respectively; two tentative assignments with $J = 47$ and 48 for $v_{30} = 2$ were weighted out in the final line list.

The set of vibrational changes to the ground state spectroscopic parameters is slightly smaller for $v_{18} = 1$ than it is for $v_{30} = 1$. In the case of $v_{30} = 2$, second changes were used for the rotational parameters and for D_{JK}; in addition, an estimate of $\Delta\Delta H_{KJ}$ was used as fixed parameter as described above.

The experimentally determined energy difference of 33.956 ± 0.020 cm^{-1} between these two states is quite well-matched by the calculated difference of 39 cm^{-1}, but less so by 18 cm^{-1} ($2 \times 99 - 180$) derived from solid-state Raman measurements (Durig et al. 2001). If the vibrational energy of $v_{30} = 2$ is close to 202 cm^{-1}, that of $v_{18} = 1$ is equally close to 168 cm^{-1}. Castro et al. (2011) studied the anharmonicity of the methyl and ethyl torsional modes. The harmonic and anharmonic energies of the methyl torsions differ by more than 15% for both conformers. The ethyl torsion was calculated to be marginally anharmonic in all models in case of the *gauche* conformer, whereas the results are less clear for the *anti* conformer. It is only slightly anharmonic in one model, but displays pronounced negative anharmonicity (i.e., the energy of $v_{30} = 2$ is *higher* than twice the energy of $v_{30} = 1$) in two others. The vibrational energy of $v_{30} = 2$ in all models is around 225 cm^{-1}, which appears to be too high and higher than the calculated anharmonic energy of 209.54 cm^{-1} for $v_{29} = 1$, which appears to

be too low. The difference between the anharmonic energies of $v_{30} = 2$ and the (harmonic) energy of $v_{18} = 1$ from Castro et al. (2011) yields values between ~63 and ~68 cm^{-1}, much larger than our experimental value of ~34 cm^{-1}. Gas phase far-infrared measurements may be the most promising way to establish the energies of the lowest vibrational states of *n*-PrCN.

5. Results of astronomical observations

Part of the observations used in this article were briefly described in Belloche et al. (2014). A detailed account of the observations, reduction, and analysis method of the full data set covering 84.1 to 114.4 GHz was reported by Belloche et al. (2016). Here we use this full data set.

As already reported in Belloche et al. (2014) on the basis of a smaller set of data, *n*-propyl cyanide is clearly detected in its vibrational ground state toward Sgr B2(N2), with about 120 lines detected with little contamination in the full EMoCA survey (Table 4 and Fig. A.1). A source size of 1.0″ was derived by Belloche et al. (2014) from Gaussian fits to the integrated intensity maps of all detected lines that suffered the least from contamination by other species. The spectrum was well-fit under the local thermodynamic equilibrium (LTE) approximation with a temperature of 150 K, a linewidth of 5 km s^{-1}, and a velocity of 73.5 km s^{-1}, leading to a column density of 1.7×10^{17} cm^{-2} after correction for the contribution of vibrationally excited states to the partition function. Please note that the column density is slightly different compared to the one reported by Belloche et al. (2014), 1.8×10^{17} cm^{-2}, because we use here a slightly different vibrational correction factor to the rotational partition function (see Table 1). The lines of the vibrational ground state of *n*-propyl cyanide detected above 110.7 GHz that were not reported in Belloche et al. (2014) are well-fit with these parameters too (see last two pages of Fig. A.1).

Using the same LTE parameters as for the vibrational ground state, we looked for lines from within vibrationally excited states of both *gauche* and *anti* propyl cyanide in the EMoCA survey of Sgr B2(N2). On the basis of this LTE model, we report the detection of one or several transitions or groups of transitions of each of the eight vibrationally excited states analyzed in the previous sections (Table 4). The parameters of the detected lines are listed in Tables B.1–B.8, and the spectra of these lines plus all those that contribute significantly to the signal detected toward Sgr B2(N2) are shown in Figs. A.2–A.9. The fact that the lines of all states, including the vibrational ground state, are well-fit with the same parameters, gives us confidence in the reliability of the identifications, even for the states with only one clearly detected line. The median size of all detected ground state and vibrationally excited state lines that do not suffer from contamination remains 1.0″, with an rms dispersion of ~0.5″ and no obvious correlation with energy level.

The population diagram of most detected lines plus those that are somewhat more contaminated but for which we have already identified and modeled most of the contaminants is shown in Fig. 6. The detected lines that consist of a blend of several transitions with significantly different upper-level energies are not used in this diagram. A fit to this diagram yields a temperature of 142 ± 4 K. As explained in Sect. 3 of Belloche et al. (2016), the uncertainty on the fitted rotation temperature is only statistical and does not include the systematic uncertainties due in particular to residual contamination by unidentified species. Our LTE model of *n*-propyl cyanide assumes a temperature of 150 K, which is consistent with the fitted rotation temperature within 2σ. The LTE model is optimized so that it never

Table 4. Number of lines of *n*-propyl cyanide detected toward Sgr B2(N2).

State	N_{det}[a]	N_{trans}[b]
$a+g\ v = 0$	116	199
$g\ v_{30} = 1$	12	16
$a\ v_{30} = 1$	9	33
$g\ v_{29} = 1$	6	8
$a\ v_{18} = 1$	3	7
$g\ v_{30} = 2$	4	4
$a\ v_{30} = 2$	3	6
$g\ v_{28} = 1$	1	2
$a\ v_{29} = 1$	1	4

Notes. [a] Number of detected lines (conservative estimate, see Sect. 3 of Belloche et al. 2016). One line of a given state may mean a group of transitions of that state that are blended together. [b] Number of transitions covered by the detected lines.

overestimates the peak temperature of any detected transition of *n*-propyl cyanide, therefore it tends to produce synthetic integrated intensities that lie below the measured ones which may suffer from residual contamination, in particular in the wings of the lines (see the location of the red crosses with respect to the other ones in Fig. 6). This is the reason why our LTE model does not use the temperature strictly derived from the population diagram.

6. Conclusion and outlook

We have analyzed the rotational spectra of the four lowest excited vibrational states of each of the two *n*-PrCN conformers in laboratory spectral recordings up to 127 GHz. We identified rovibrational interactions between $v_{18} = 1$ and $v_{30} = 2$ of the *anti* conformer. We modeled the perturbations with one Coriolis and one Fermi parameter and determined the energy difference between these states quite accurately.

The resulting spectroscopic parameters enabled us to identify transitions of each excited vibrational state in our ALMA 3 mm molecular line survey of Sgr B2(N2). The emission of all states is well reproduced with the model parameters we obtained previously for the ground vibrational state.

The emission caused by molecules in excited vibrational states may be used to infer (far-) infrared pumping in a given source. Our results concerning vibrational states of *n*-PrCN suggest that far-infrared pumping is, at least, not so important that it alters the apparent vibrational temperature in the region of Sgr B2(N2) which is probed by the *n*-PrCN emission. We note that in Sgr B2(N2) there are molecules which are better suited to investigate (far-) infrared pumping, even more so in other sources in which *n*-PrCN has not yet been detected.

If LTE is a reasonable assumption, transitions of molecules in excited vibrational states may be used to constrain the rotational temperature if ground state rotational transitions cover an energy range that is too narrow to constrain it. This may be useful for linear molecules or for fairly light molecules; for example, we used transitions of torsionally excited methanethiol to constrain the rotational temperature of this molecule (Müller et al. 2016b).

Observations with deeper integration may make it possible to identify even higher vibrationally excited states of *n*-PrCN as long as the confusion limit is not reached. In addition, the sensitivity of our current ALMA data may be sufficient to identify
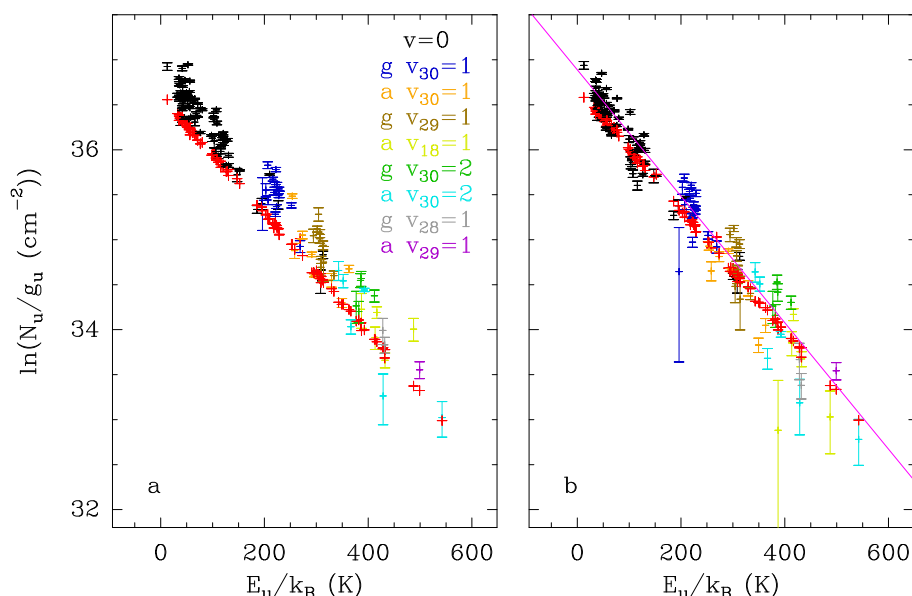
Fig. 6. Population diagram of *n*-propyl cyanide toward Sgr B2(N2). Only the lines that are clearly detected and do not suffer too much from contamination by other species are displayed. The observed data points are shown in various colors (except red) as indicated in the upper right corner of panel **a)** while the synthetic populations are shown in red. No correction is applied in panel **a)**. In panel **b)**, the optical depth correction has been applied to both the observed and synthetic populations and the contamination by all other species included in the full model has been removed from the observed data points. The purple line is a linear fit to the observed populations (in linear-logarithmic space). The derived rotation temperature is 142 ± 4 K.

the ^{13}C isotopomers of this molecule because the ^{12}C/^{13}C ratio of many molecules in Sgr B2(N2) was determined to be close to 25 (Belloche et al. 2016; Müller et al. 2016b; Margulès et al. 2016).

Predictions of the rotational spectra of the four lowest excited vibrational states of both conformers of *n*-PrCN will be available in the catalog section[4] of the ascii version of the Cologne Database for Molecular Spectroscopy (CDMS; Müller et al. 2001, 2005) as well as in the Virtual Atomic and Molecular Data Centre (VAMDC; Dubernet et al. 2010, 2016) compatible version of the CDMS[5] (Endres et al. 2016). The complete line, parameter, and fit files along with auxiliary files will be deposited in the Spectroscopy Data section of the CDMS[6].

Future laboratory work will focus on analyzing the submillimeter spectra to extend assignments for the eight vibrationally excited states of the present investigation. This work has begun, should improve spectroscopic parameters considerably, and will be useful for potential assignments of radio astronomical spectra at higher frequencies. Furthermore, we will try to assign higher excited vibrational states; initial assignments exist for some combination and overtone states. Such states may be observable in more sensitive ALMA data of Sgr B2(N).

---

[4] Website: http://www.astro.uni-koeln.de/cdms/entries/
[5] http://cdms.ph1.uni-koeln.de/cdms/portal
[6] http://www.astro.uni-koeln.de/site/vorhersagen/daten/n-PrCN/

References

Belloche, A., Garrod, R. T., Müller, H. S. P., et al. 2009, A&A, 499, 215

Belloche, A., Müller, H. S. P., Menten, K. M., Schilke, P., & Comito, C. 2013, A&A, 559, A47

Belloche, A., Garrod, R. T., Müller, H. S. P., & Menten, K. M. 2014, Science, 345, 1584

Belloche, A., Müller, H. S. P., Garrod, R. T., & Menten, K. M. 2016, A&A, 587, A91

Bossa, J.-B., Ordu, M. H., Müller, H. S. P., Lewen, F., & Schlemmer, S. 2014, A&A, 570, A12

Castro, M. E., Muñoz-Caro, C., & Niño, A. 2011, Int. J. Quant. Chem., 111, 3681

Charles, S. W., Cullen, F. C., & Owen, N. L. 1976, J. Mol. Struct., 34, 219

Crowder, G. A. 1987, J. Mol. Struct., 158, 229

Demaison, J., & Dreizler, H. 1982, Z. Naturforsch. A, 37, 199

Dubernet, M. L., Boudon, V., Culhane, J. L., et al. 2010, J. Quant. Spectrosc. Radiat. Transfer, 111, 2151

Dubernet, M. L., Antony, B. K., Ba, Y. A., et al. 2016, J. Phys. B, 49, 074003

Durig, J. R., Drew, B. R., Koomer, A., & Bell, S. 2001, Phys. Chem. Chem. Phys., 3, 766

Endres, C. P., Schlemmer, S., Schilke, P., Stutzki, J., & Müller, H. S. P. 2016, J. Mol. Spectrosc., 327, 95

Hirota, E. 1962, J. Chem. Phys., 37, 2918

Laurie, V. W. 1959, J. Chem. Phys., 31, 1500

Margulès, L., Belloche, A., Müller, H. S. P., et al. 2016, A&A, 590, A93

Müller, H. S. P., Miller, C. E., & Cohen, E. A. 1997a, J. Chem. Phys., 107, 8292

Müller, H. S. P., Sørensen, G. O., Birk, M., & Friedl, R. R. 1997b, J. Mol. Spectrosc., 186, 177

Müller, H. S. P., Thorwirth, S., Roth, D. A., & Winnewisser, G. 2001, A&A, 370, L49

Müller, H. S. P., Schlöder, F., Stutzki, J., & Winnewisser, G. 2005, J. Mol. Struct., 742, 215

Müller, H. S. P., Coutens, A., Walters, A., Grabow, J.-U., & Schlemmer, S. 2011, J. Mol. Spectrosc., 267, 100

Müller, H. S. P., Brown, L. R., Drouin, B. J., et al. 2015, J. Mol. Spectrosc., 312, 22

Müller, H. S. P., Drouin, B. J., Pearson, J. C., et al. 2016a, A&A, 586, A17

Müller, H. S. P., Belloche, A., Xu, L.-H., et al. 2016b, A&A, 587, A92

Pickett, H. M. 1991, J. Mol. Spectrosc., 148, 371

Schmiedeke, A., Schilke, P., Möller, T., et al. 2016, A&A, 588, A143

Traetteberg, M., Bakken, P., & Hopf, H. 2000, J. Mol. Struct., 556, 189

Vormann, K., & Dreizler, H. 1988, Z. Naturforsch. A, 43, 338

Walters, A., Schäfer, M., Ordu, M. H., et al. 2015, J. Mol. Spectrosc., 314, 6

Wlodarczak, G., Martinache, L., Demaison, J., Marstokk, K.-M., & Møllendal, H. 1988, J. Mol. Spectrosc., 127, 178

Wlodarczak, G., Martinache, L., Demaison, J., Marstokk, K.-M., & Møllendal, H. 1991, J. Mol. Spectrosc., 146, 224

Appendix A: Complementary figures

Figures A.1–A.9 show the transitions of *n*-propyl cyanide that are covered by the EMoCA survey and contribute significantly to the signal detected toward Sgr B2(N2).
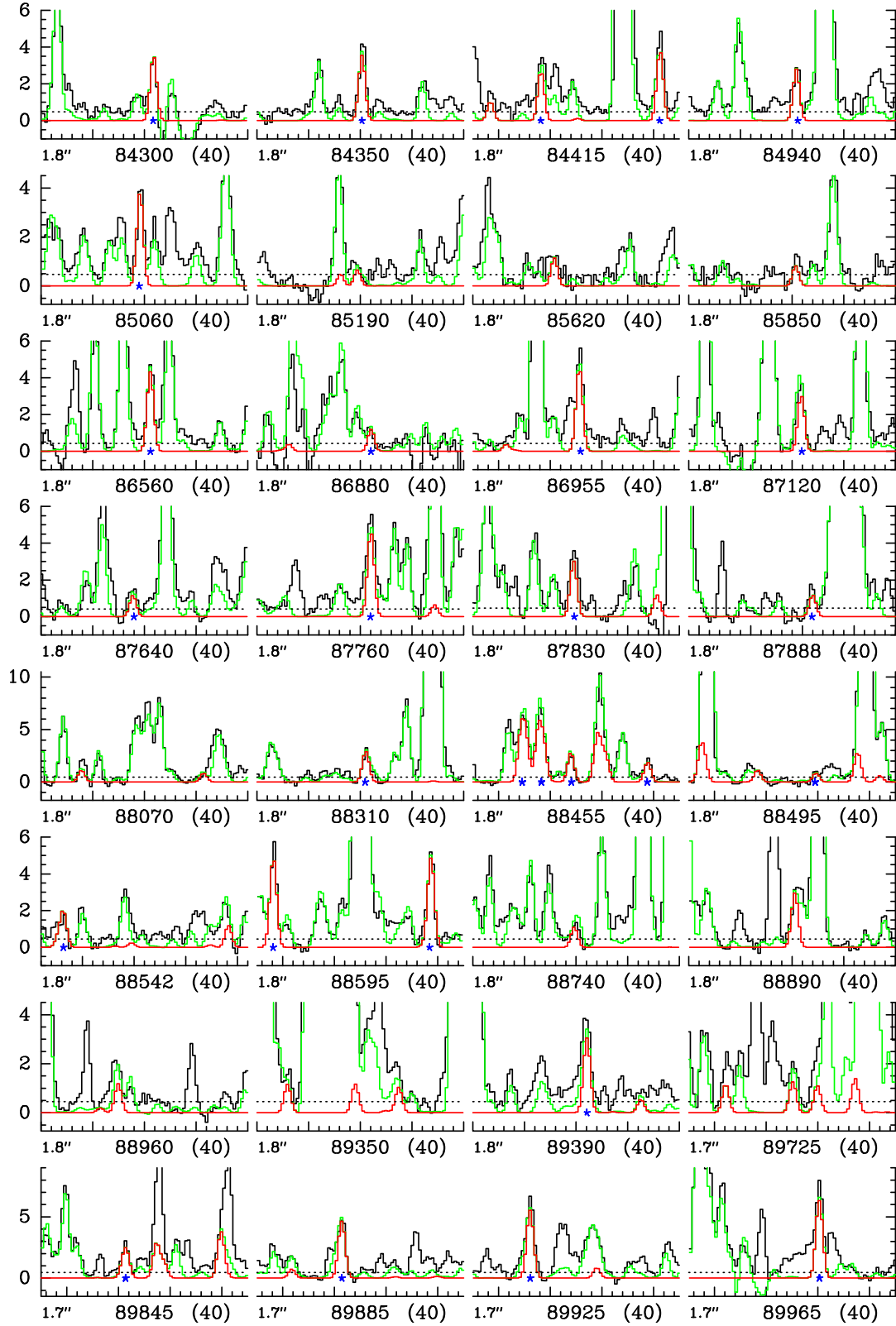

Fig. A.1. Transitions of *n*-C$_3$H$_7$CN, $v = 0$ covered by our ALMA survey. The best-fit LTE synthetic spectrum of *n*-C$_3$H$_7$CN is displayed in red and overlaid on the observed spectrum of Sgr B2(N2) shown in black. The green synthetic spectrum contains the contributions of all molecules identified in our survey so far, including the species shown in red. The central frequency and width are indicated in MHz below each panel. The angular resolution (HPBW) is also indicated. The y-axis is labeled in brightness temperature units (K). The dotted line indicates the 3σ noise level. Blue stars indicate the lines of *n*-C$_3$H$_7$CN that are counted as detected in Table 4.
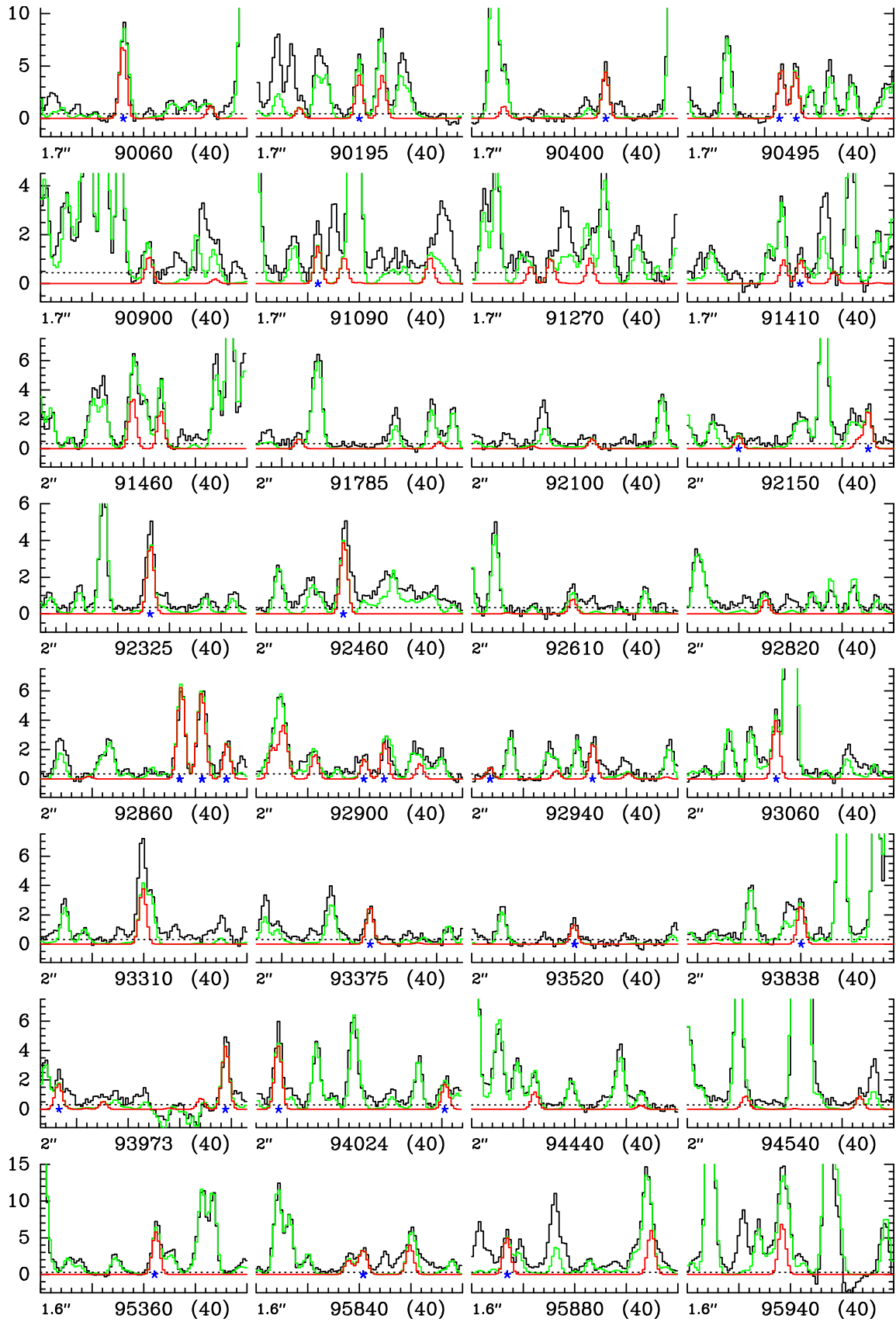
Fig. A.1. continued.
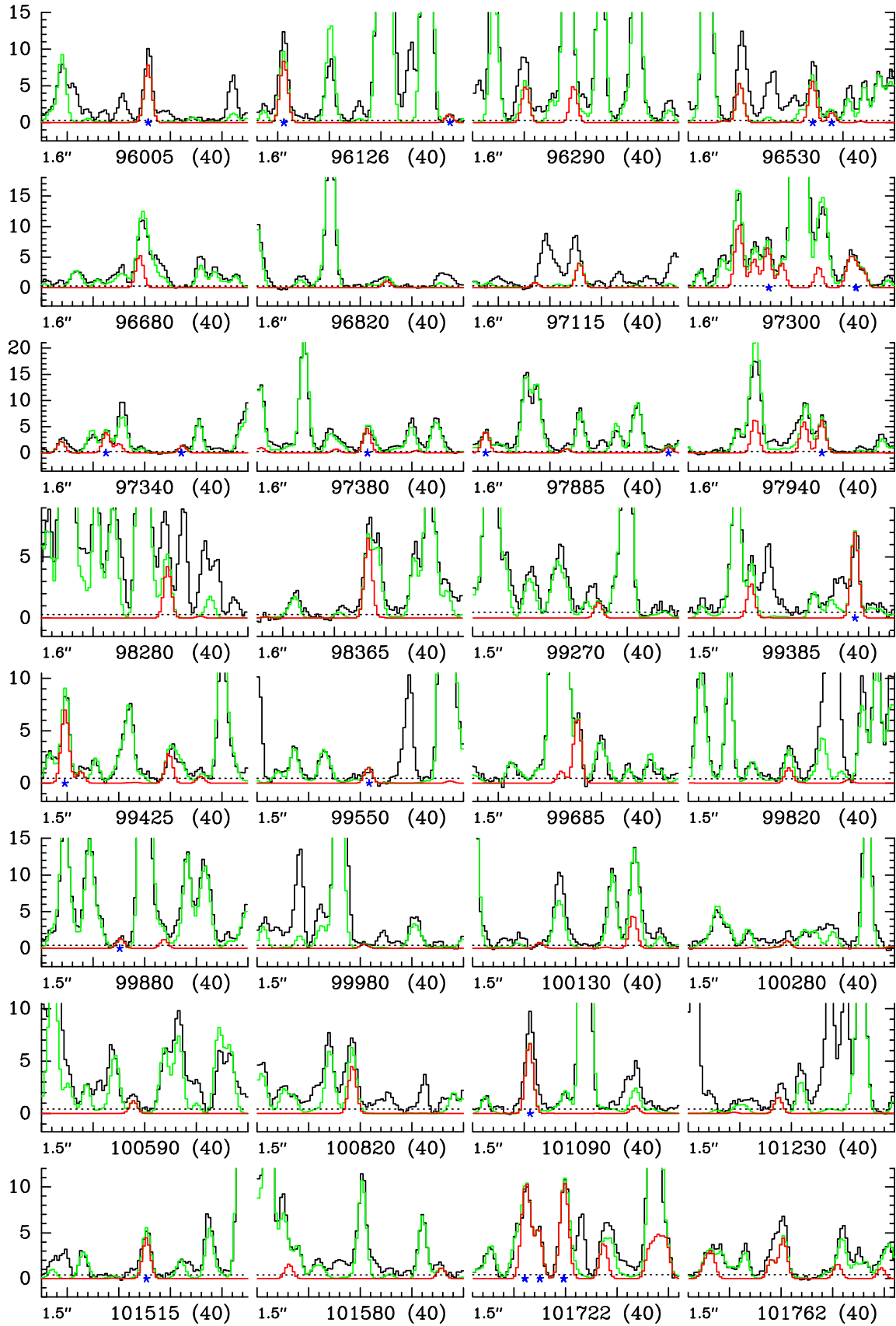
Fig. A.1. continued.
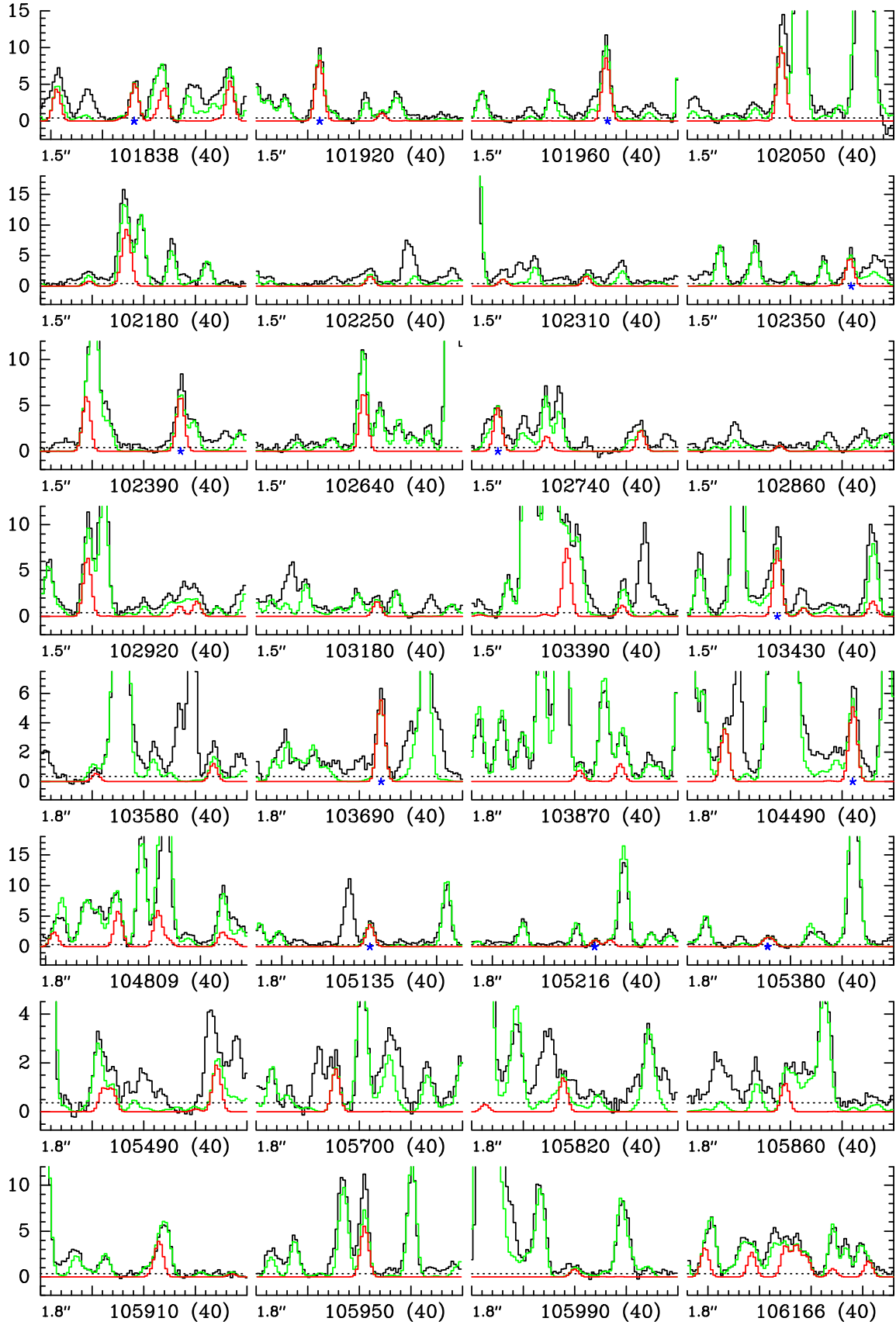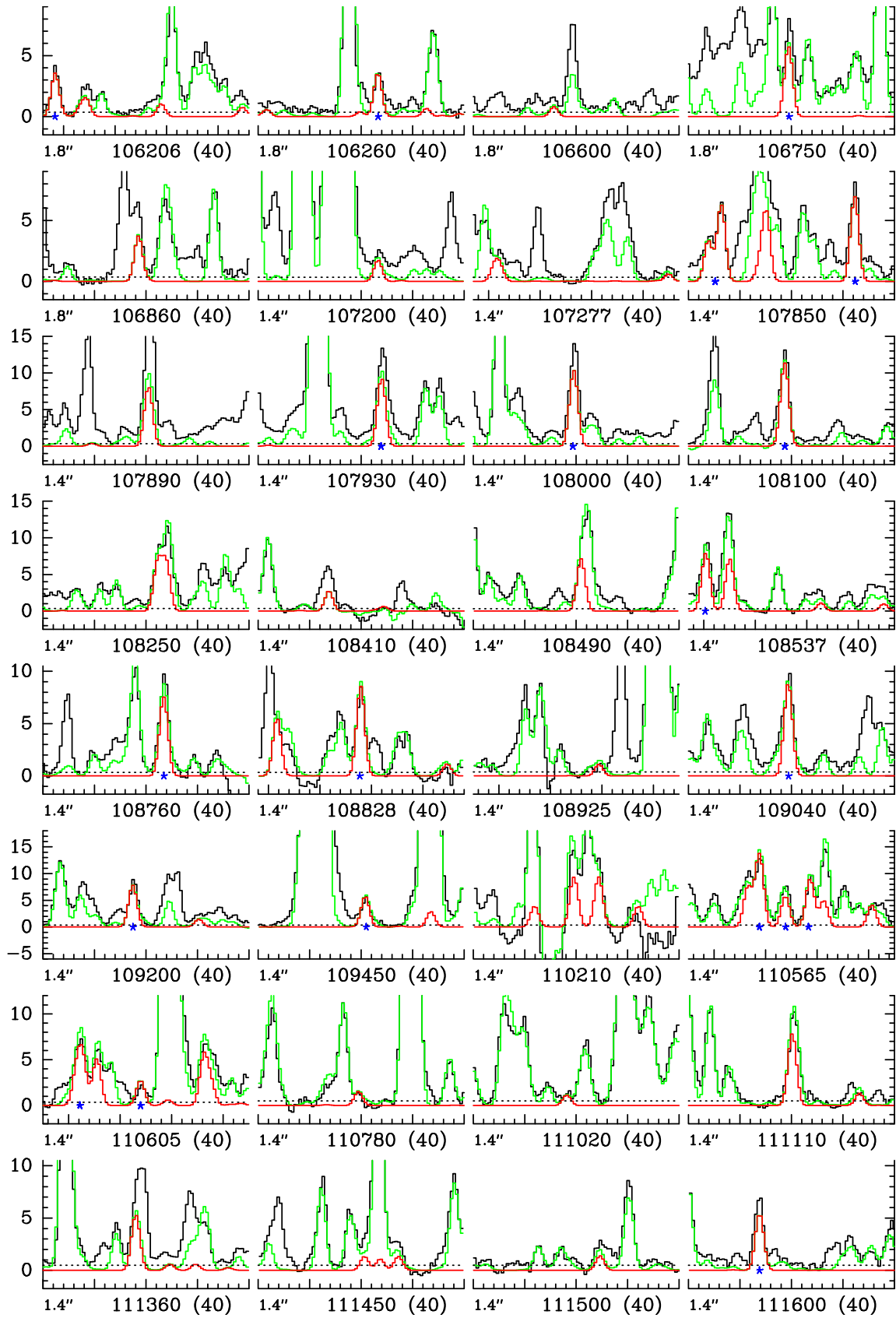
Fig. A.1. continued.
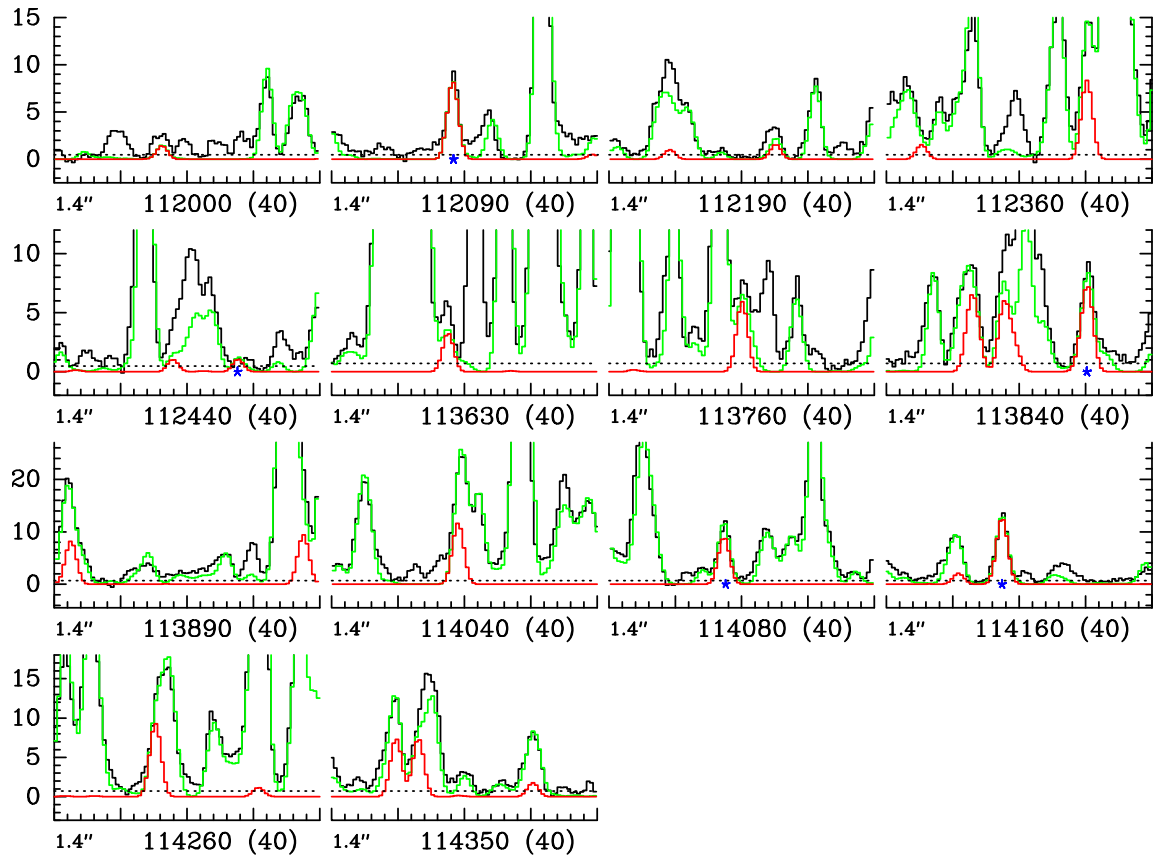
Fig. A.1. continued.
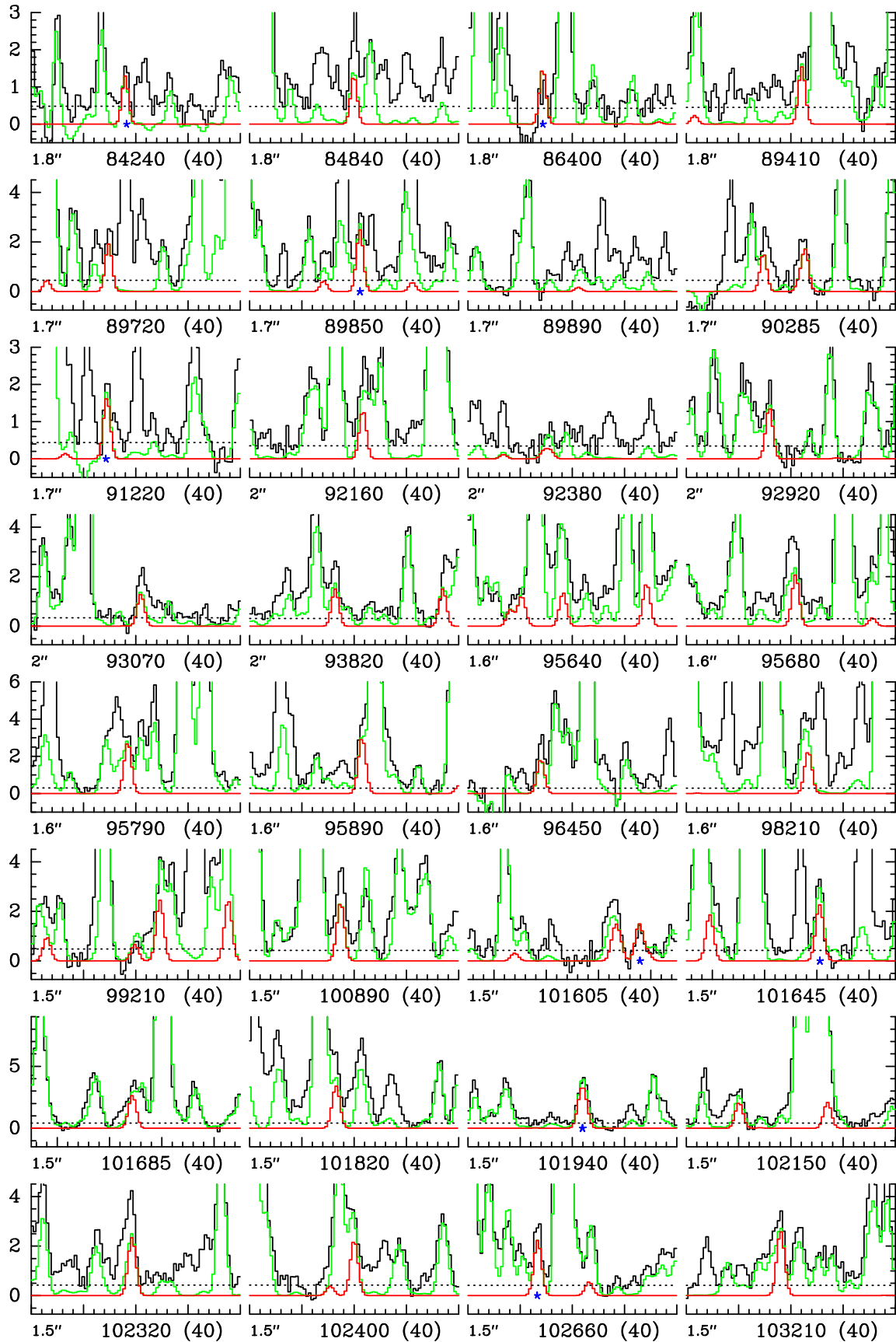
Fig. A.1. continued.

Fig. A.2. Same as Fig. A.1 for *gauche n*-C$_3$H$_7$CN, $v_{30} = 1$.
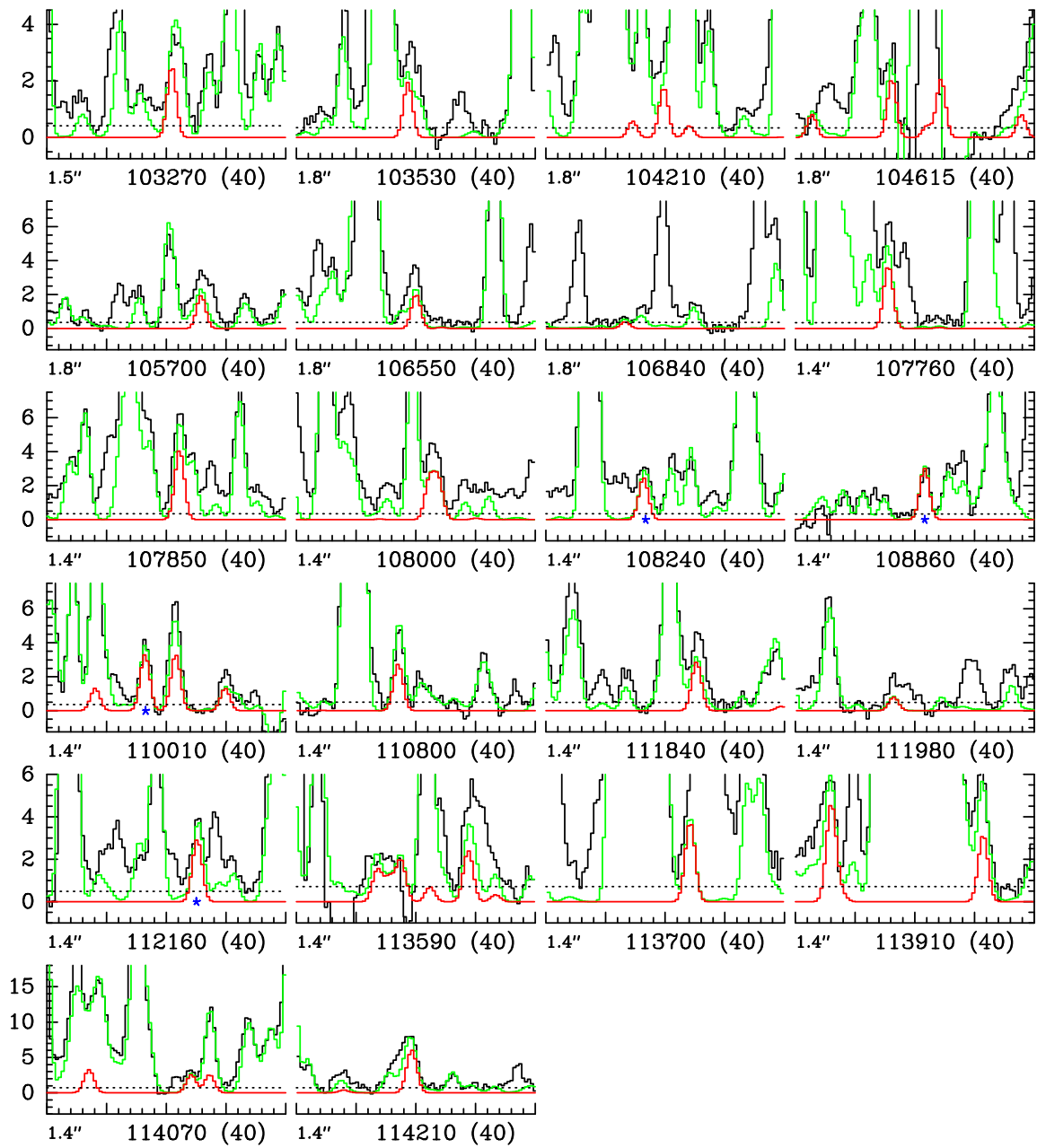
Fig. A.2. continued.
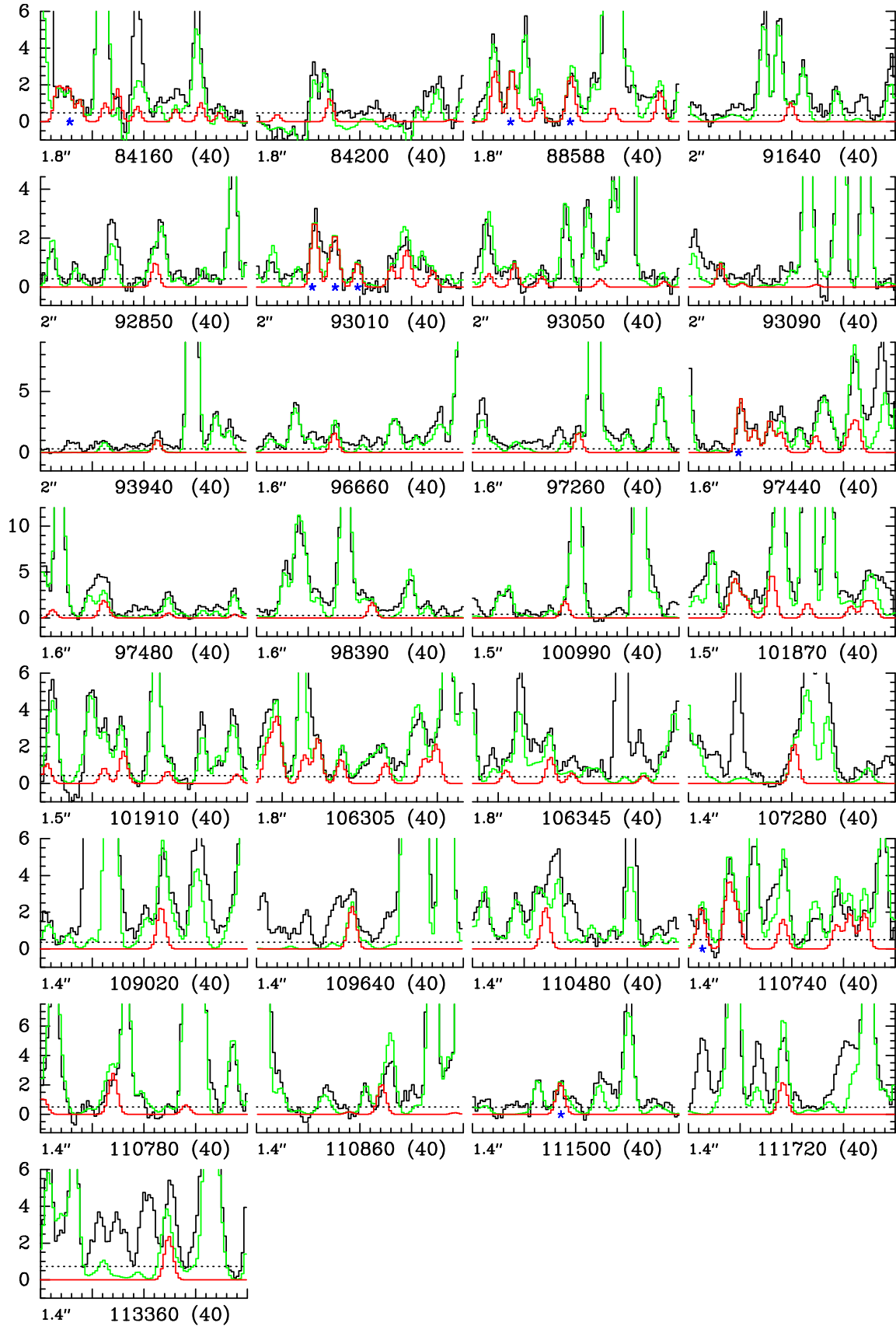
Fig. A.3. Same as Fig. A.1 for *anti n*-C$_3$H$_7$CN, $v_{30} = 1$.
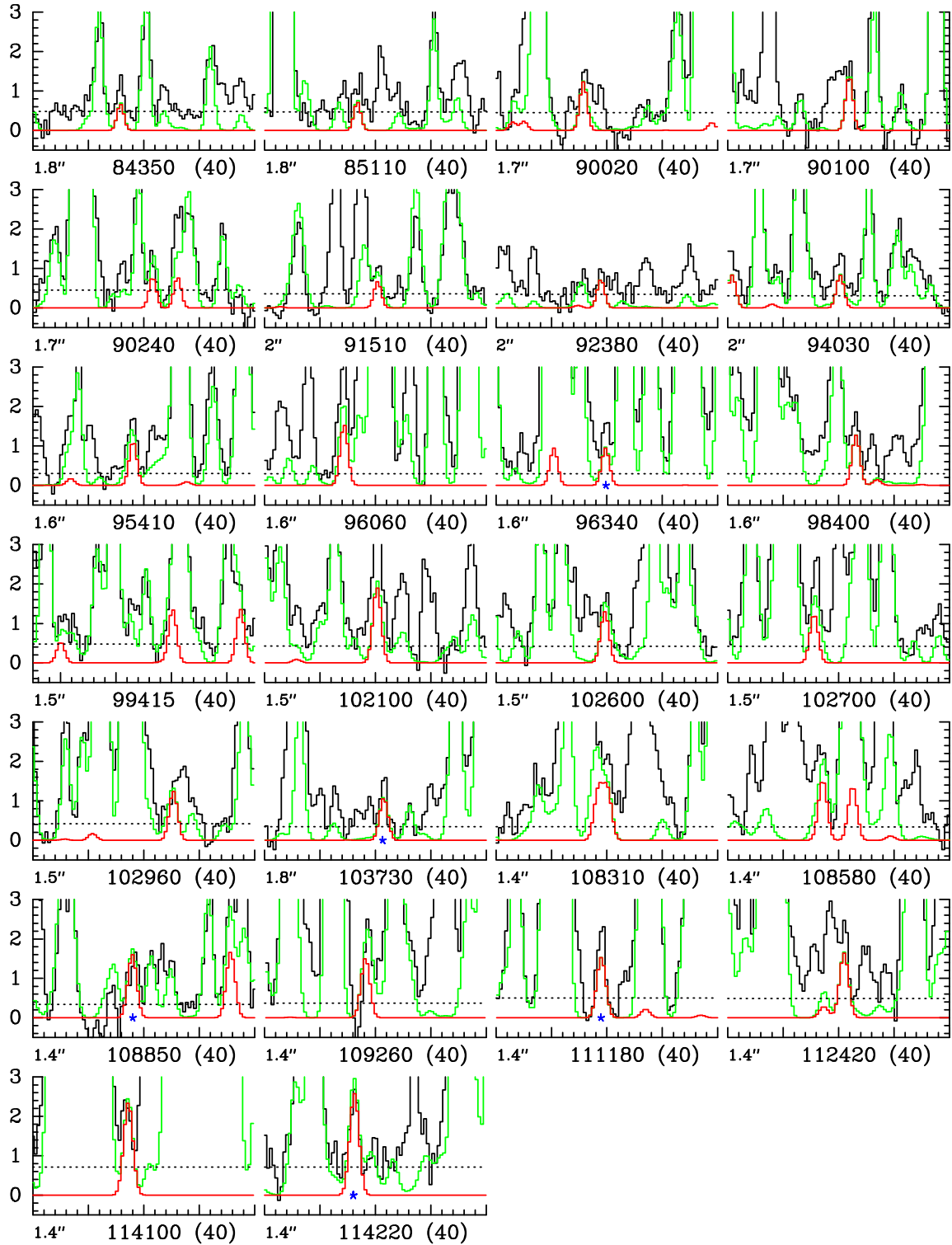
Fig. A.4. Same as Fig. A.1 for *gauche n*-C$_3$H$_7$CN, v_{29} = 1.
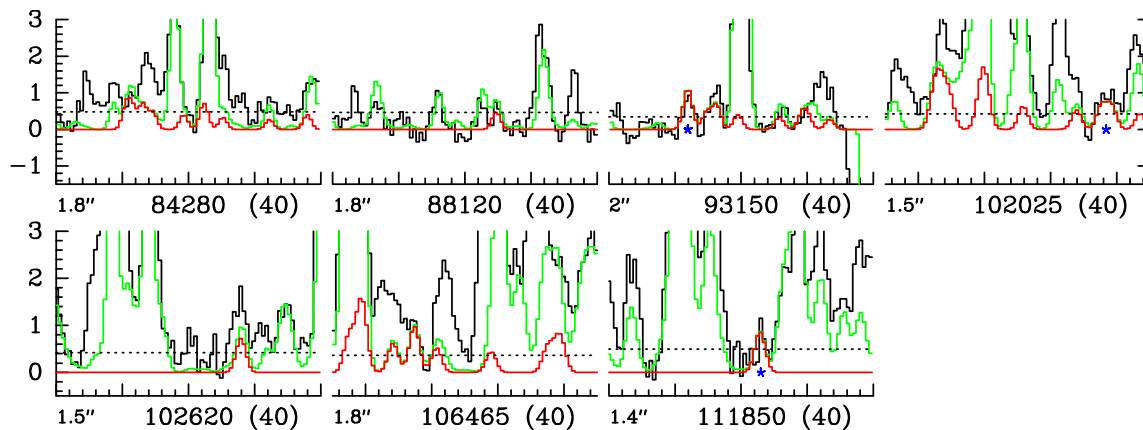
Fig. A.5. Same as Fig. A.1 for *anti n*-C$_3$H$_7$CN, $v_{18} = 1$.
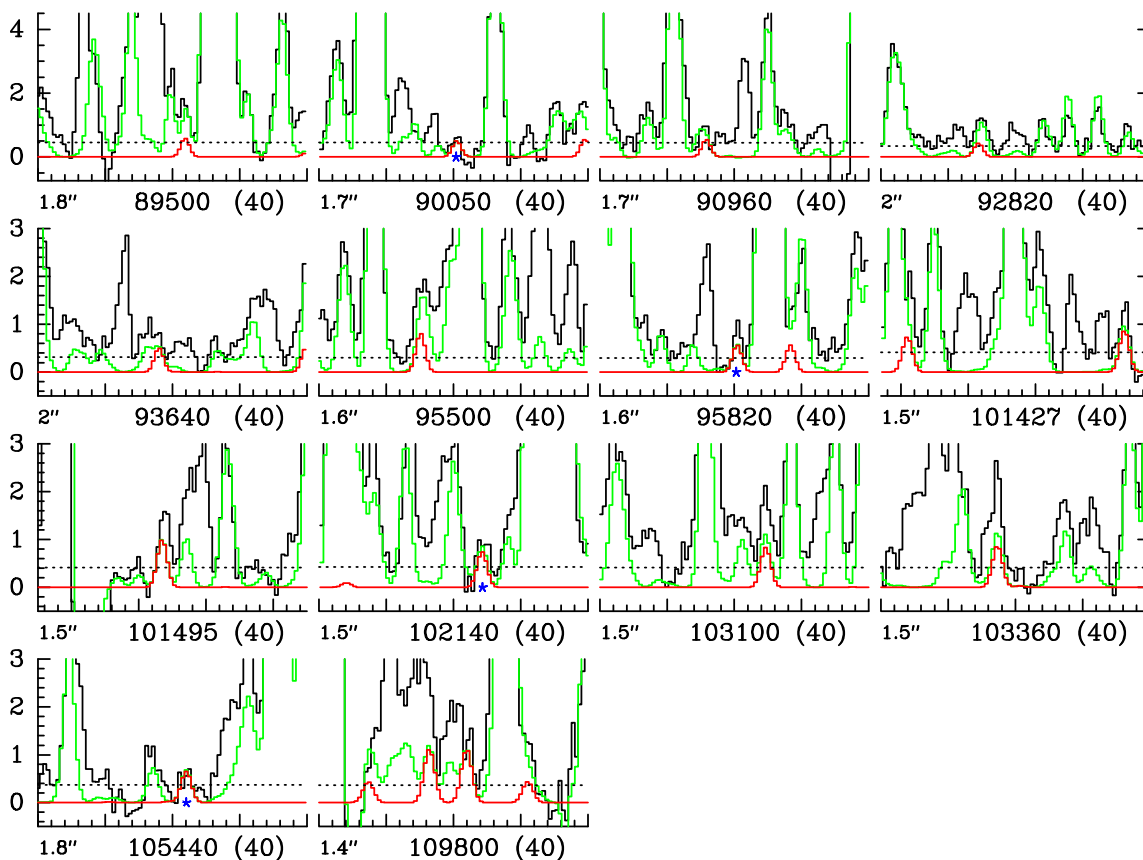
Fig. A.6. Same as Fig. A.1 for *gauche n*-C$_3$H$_7$CN, $v_{30} = 2$.
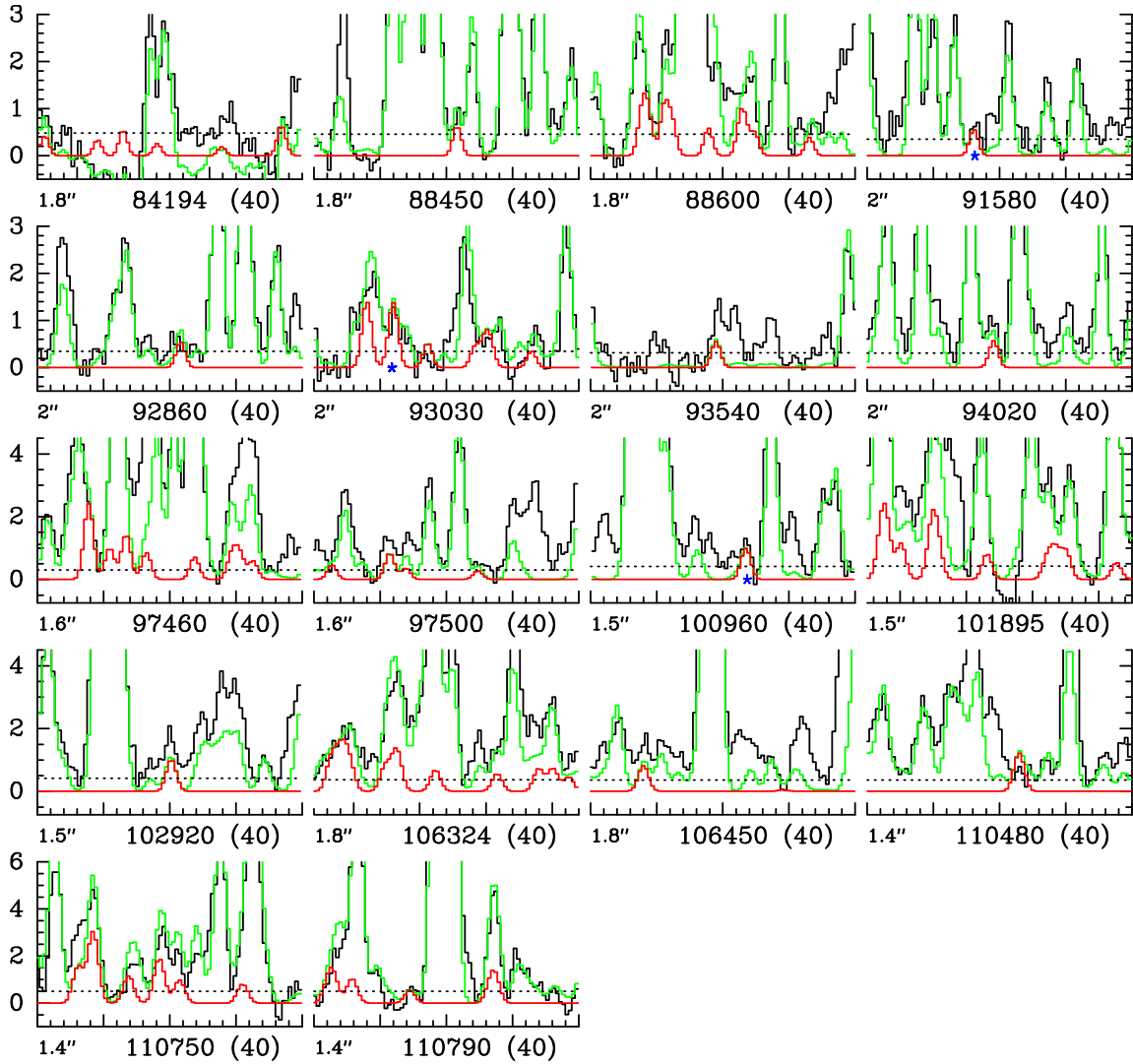
Fig. A.7. Same as Fig. A.1 for *anti* n-C$_3$H$_7$CN, $v_{30} = 2$.
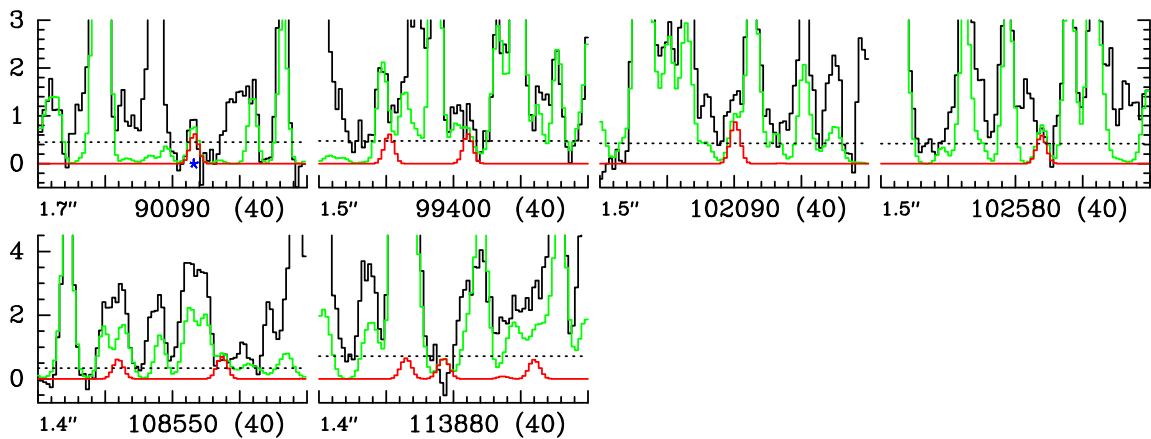

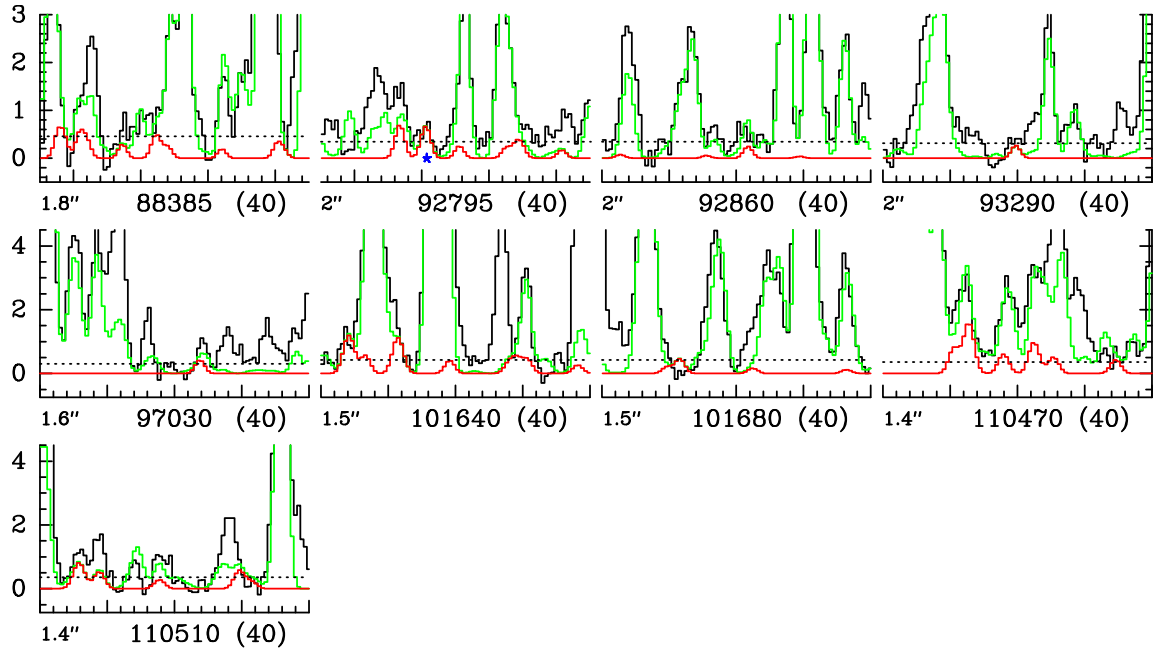**Fig. A.8.** Same as Fig. A.1 for *gauche* n-C$_3$H$_7$CN, $v_{28} = 1$.

Fig. A.9. Same as Fig. A.1 for *anti* *n*-C$_3$H$_7$CN, $v_{29} = 1$.

Appendix B: Complementary tables

Tables B.1–B.8 list the transitions from within vibrationally excited states of *n*-propyl cyanide that are detected toward Sgr B2(N2), meaning that are above the 3σ level and do not suffer much from contamination by other species.

Table B.1. Selection of lines of *gauche* propyl cyanide $v_{30} = 1$ covered by the EMoCA survey of Sgr B2(N2).

Transition[a]	Frequency (MHz)	Unc.[b] (kHz)	E_{up}[c] (K)	g_{up}[d]	A_{ul}[e] $(10^{-5} s^{-1})$	σ[f] (mK)	τ_{peak}[g]	Frequency range[h] (MHz)	(MHz)	I_{obs}[i] (K km s^{-1})	I_{mod}[j] (K km s^{-1})	I_{all}[k]
$14_{4,11}-13_{4,10}$	84 237.836	1	203	58	3.3	158	0.041	84 236.8	84 239.7	9.1(7)*	6.9	6.8
$14_{2,12}-13_{2,11}$	86 394.181	1	199	58	3.8	142	0.044	86 392.9	86 395.8	5.9(6)	8.0	8.1
$15_{7,9}-14_{7,8}$	89 850.897	1	218	62	3.4	149	0.073	89 849.9	89 852.4	19.1(5)*	12.9	14.7
$15_{7,8}-14_{7,7}$	89 851.023	1	218	62	3.4	–	–	–	–	–	–	–
$15_{4,11}-14_{4,10}$	91 214.307	1	207	62	4.3	149	0.047	91 213.1	91 215.6	10.6(5)*	8.5	9.3
$17_{13,4}-16_{13,3}$	101 617.584	1	269	70	2.6	141	0.036	101 616.2	101 619.6	8.2(5)*	9.0	9.1
$17_{13,5}-16_{13,4}$	101 617.584	1	269	70	2.6	–	–	–	–	–	–	–
$17_{11,6}-16_{11,5}$	101 650.360	1	252	70	3.7	141	0.056	101 648.9	101 652.3	18.5(5)*	12.0	17.7
$17_{11,7}-16_{11,6}$	101 650.360	1	252	70	3.7	–	–	–	–	–	–	–
$17_{7,11}-16_{7,10}$	101 941.402	1	228	70	5.3	141	0.081	101 939.5	101 944.4	29.6(6)*	20.5	26.3
$17_{7,10}-16_{7,9}$	101 942.099	1	228	70	5.3	–	–	–	–	–	–	–
$17_{5,12}-16_{5,11}$	102 653.203	1	220	70	6.0	141	0.055	102 651.6	102 655.0	18.5(5)*	12.0	12.7
$18_{6,13}-17_{6,12}$	108 236.201	1	228	74	6.8	115	0.056	108 235.3	108 238.2	20.7(4)*	12.4	16.9
$19_{1,18}-18_{1,17}$	108 861.471	1	221	78	7.7	115	0.070	108 859.5	108 863.9	18.3(5)*	16.6	17.6
$20_{1,20}-19_{1,19}$	110 006.258	1	223	82	8.0	123	0.074	110 004.6	110 008.5	22.2(5)*	17.9	20.7
$19_{3,17}-18_{3,16}$	112 165.026	1	224	78	8.3	166	0.068	112 163.4	112 166.8	25.3(6)*	15.6	21.4

Notes. [a] Quantum numbers of the upper and lower levels. [b] Frequency uncertainty. [c] Upper level energy. [d] Upper level degeneracy. [e] Einstein coefficient for spontaneous emission. [f] Measured rms noise level. [g] Peak opacity of the synthetic line. [h] Frequency range over which the emission was integrated. [i] Integrated intensity of the observed spectrum in brightness temperature scale. The statistical standard deviation is given in parentheses in unit of the last digit. Values marked with a star are used in the population diagram shown in Fig. 6. [j] Integrated intensity of the synthetic spectrum of the selected state. [k] Integrated intensity of the model that contains the contribution of all identified molecules, including *n*-propyl cyanide and its vibrationally excited states.

Table B.2. Selection of lines of *anti* propyl cyanide $v_{30} = 1$ covered by the EMoCA survey of Sgr B2(N2).

Transition[a]	Frequency (MHz)	Unc.[b] (kHz)	E_{up}[c] (K)	g_{up}[d]	A_{ul}[e] (10^{-5} s^{-1})	σ[f] (mK)	τ_{peak}[g]	Frequency range[h] (MHz)	(MHz)	I_{obs}[i] (K km s^{-1})	I_{mod}[j] (K km s^{-1})	I_{all}[k]
$19_{6,14}-18_{6,13}$	84 142.973	1	276	39	4.9	158	0.063	84 142.5	84 148.8	30.7(10)	30.5	29.0
$19_{6,13}-18_{6,12}$	84 142.973	1	276	39	4.9	–	–	–	–	–	–	–
$19_{7,12}-18_{7,11}$	84 144.088	1	289	39	4.7	–	–	–	–	–	–	–
$19_{7,13}-18_{7,12}$	84 144.088	1	289	39	4.7	–	–	–	–	–	–	–
$19_{5,15}-18_{5,14}$	84 145.416	1	265	39	5.0	–	–	–	–	–	–	–
$19_{5,14}-18_{5,13}$	84 145.420	1	265	39	5.0	–	–	–	–	–	–	–
$19_{8,11}-18_{8,10}$	84 147.434	1	304	39	4.5	–	–	–	–	–	–	–
$19_{8,12}-18_{8,11}$	84 147.434	1	304	39	4.5	–	–	–	–	–	–	–
$20_{5,16}-19_{5,15}$	88 575.296	1	269	41	5.9	153	0.088	88 574.2	88 576.7	16.9(6)	16.0	16.6
$20_{5,15}-19_{5,14}$	88 575.302	1	269	41	5.9	–	–	–	–	–	–	–
$20_{8,12}-19_{8,11}$	88 575.904	1	308	41	5.3	–	–	–	–	–	–	–
$20_{8,13}-19_{8,12}$	88 575.904	1	308	41	5.3	–	–	–	–	–	–	–
$20_{4,17}-19_{4,16}$	88 586.378	1	261	41	6.1	153	0.079	88 585.0	88 588.9	21.6(7)	16.4	23.7
$20_{4,16}-19_{4,15}$	88 586.967	1	261	41	6.1	–	–	–	–	–	–	–
$20_{10,10}-19_{10,9}$	88 587.381	1	344	41	4.7	–	–	–	–	–	–	–
$20_{10,11}-19_{10,10}$	88 587.381	1	344	41	4.7	–	–	–	–	–	–	–
$21_{6,16}-20_{6,15}$	93 001.000	1	285	43	6.7	117	0.104	92 999.3	93 002.2	17.6(5)*	14.4	14.6
$21_{6,15}-20_{6,14}$	93 001.000	1	285	43	6.7	–	–	–	–	–	–	–
$21_{7,14}-20_{7,13}$	93 001.254	1	298	43	6.5	–	–	–	–	–	–	–
$21_{7,15}-20_{7,14}$	93 001.254	1	298	43	6.5	–	–	–	–	–	–	–
$21_{8,13}-20_{8,12}$	93 004.322	1	313	43	6.3	117	0.083	93 003.2	93 007.1	15.4(5)	15.4	16.3
$21_{8,14}-20_{8,13}$	93 004.322	1	313	43	6.3	–	–	–	–	–	–	–
$21_{5,17}-20_{5,16}$	93 005.356	1	274	43	6.9	–	–	–	–	–	–	–
$21_{5,16}-20_{5,15}$	93 005.365	1	274	43	6.9	–	–	–	–	–	–	–
$21_{9,12}-20_{9,11}$	93 009.378	1	329	43	6.0	117	0.038	93 008.1	93 011.0	6.0(5)*	5.4	6.0
$21_{9,13}-20_{9,12}$	93 009.378	1	329	43	6.0	–	–	–	–	–	–	–
$22_{7,15}-21_{7,14}$	97 429.823	1	302	45	7.6	100	0.119	97 428.0	97 431.4	23.4(4)*	24.0	24.1
$22_{7,16}-21_{7,15}$	97 429.823	1	302	45	7.6	–	–	–	–	–	–	–
$22_{6,17}-21_{6,16}$	97 430.109	1	290	45	7.8	–	–	–	–	–	–	–
$22_{6,16}-21_{6,15}$	97 430.109	1	290	45	7.8	–	–	–	–	–	–	–
$25_{9,16}-24_{9,15}$	110 722.260	1	349	51	10.8	166	0.051	110 721.0	110 724.5	11.8(6)*	11.6	16.2
$25_{9,17}-24_{9,16}$	110 722.260	1	349	51	10.8	–	–	–	–	–	–	–
$25_{2,23}-24_{2,22}$	111 496.841	2	273	51	12.6	166	0.050	111 495.2	111 499.1	14.5(6)*	11.5	14.9

Notes. See Table B.1.

Table B.3. Selection of lines of *gauche* propyl cyanide $v_{29} = 1$ covered by the EMoCA survey of Sgr B2(N2).

Transition[a]	Frequency (MHz)	Unc.[b] (kHz)	E_{up}[c] (K)	g_{up}[d]	A_{ul}[e] (10^{-5} s^{-1})	σ[f] (mK)	τ_{peak}[g]	Frequency range[h] (MHz)	(MHz)	I_{obs}[i] (K km s^{-1})	I_{mod}[j] (K km s^{-1})	I_{all}[k]
$16_{6,10}-15_{6,9}$	96 339.593	1	309	66	4.6	155	0.025	96 338.6	96 341.0	5.7(5)*	4.8	5.2
$18_{1,17}-17_{1,16}$	103 731.332	2	307	74	6.6	114	0.035	103 729.6	103 733.1	8.6(4)*	5.7	6.2
$15_{8,7}-15_{7,8}$	105 942.286	3	314	62	1.3	123	0.011	105 941.0	105 943.9	2.2(4)*	1.7	2.5
$15_{8,8}-15_{7,9}$	105 942.502	3	314	62	1.3	–	–	–	–	–	–	–
$18_{2,16}-17_{2,15}$	108 847.764	2	309	74	7.6	115	0.036	108 846.3	108 849.7	10.4(4)*	8.6	9.9
$18_{4,14}-17_{4,13}$	111 178.807	2	313	74	7.9	166	0.036	111 177.2	111 180.6	11.9(6)*	8.0	8.1
$19_{8,12}-18_{8,11}$	114 215.993	2	334	78	7.4	242	0.058	114 214.1	114 218.0	16.7(9)*	14.0	17.4
$19_{8,11}-18_{8,10}$	114 216.118	2	334	78	7.4	–	–	–	–	–	–	–

Notes. See Table B.1.

Table B.4. Selection of lines of *anti* propyl cyanide $v_{18} = 1$ covered by the EMoCA survey of Sgr B2(N2).

Transition[a]	Frequency (MHz)	Unc.[b] (kHz)	E_{up}[c] (K)	g_{up}[d]	A_{ul}[e] (10^{-5} s^{-1})	σ[f] (mK)	τ_{peak}[g]	Frequency range[h] (MHz)	(MHz)	I_{obs}[i] (K km s^{-1})	I_{mod}[j] (K km s^{-1})	I_{all}[k]
$21_{6,16}-20_{6,15}$	93 141.752	1	426	43	6.7	117	0.041	93 140.5	93 143.4	5.4(5)⋆	6.1	6.1
$21_{6,15}-20_{6,14}$	93 141.752	1	426	43	6.7	–	–	–	–	–	–	–
$21_{7,14}-20_{7,13}$	93 141.838	1	439	43	6.5	–	–	–	–	–	–	–
$21_{7,15}-20_{7,14}$	93 141.838	1	439	43	6.5	–	–	–	–	–	–	–
$23_{4,20}-22_{4,19}$	102 037.514	1	417	47	9.4	141	0.018	102 036.2	102 040.6	9.5(6)⋆	6.9	7.2
$23_{4,19}-22_{4,18}$	102 039.055	1	417	47	9.4	–	–	–	–	–	–	–
$25_{1,24}-24_{1,23}$	111 852.657	2	413	51	12.7	166	0.020	111 851.3	111 854.7	4.6(6)⋆	4.5	4.8

Notes. See Table B.1.

Table B.5. Selection of lines of *gauche* propyl cyanide $v_{30} = 2$ covered by the EMoCA survey of Sgr B2(N2).

Transition[a]	Frequency (MHz)	Unc.[b] (kHz)	E_{up}[c] (K)	g_{up}[d]	A_{ul}[e] (10^{-5} s^{-1})	σ[f] (mK)	τ_{peak}[g]	Frequency range[h] (MHz)	(MHz)	I_{obs}[i] (K km s^{-1})	I_{mod}[j] (K km s^{-1})	I_{all}[k]
$15_{5,10}-14_{5,9}$	90 050.371	1	377	62	3.9	149	0.014	90 049.2	90 051.6	3.1(5)⋆	2.6	2.6
$16_{6,11}-15_{6,10}$	95 820.263	1	385	66	4.6	100	0.015	95 818.8	95 821.8	4.8(4)⋆	3.0	3.1
$17_{5,13}-16_{5,12}$	102 144.113	1	386	70	5.9	141	0.018	102 142.7	102 146.1	6.5(5)⋆	4.0	4.9
$17_{3,14}-16_{3,13}$	105 441.876	1	382	70	6.9	123	0.021	105 440.3	105 443.7	3.8(5)⋆	3.5	3.7

Notes. See Table B.1.

Table B.6. Selection of lines of *anti* propyl cyanide $v_{30} = 2$ covered by the EMoCA survey of Sgr B2(N2).

Transition[a]	Frequency (MHz)	Unc.[b] (kHz)	E_{up}[c] (K)	g_{up}[d]	A_{ul}[e] (10^{-5} s^{-1})	σ[f] (mK)	τ_{peak}[g]	Frequency range[h] (MHz)	(MHz)	I_{obs}[i] (K km s^{-1})	I_{mod}[j] (K km s^{-1})	I_{all}[k]
$21_{1,21}-20_{1,20}$	91 576.003	2	343	43	6.9	117	0.021	91 575.1	91 577.5	4.0(4)⋆	2.8	2.9
$21_{8,13}-20_{8,12}$	93 021.503	2	411	43	6.2	117	0.055	93 020.3	93 023.3	8.6(5)	7.9	10.2
$21_{8,14}-20_{8,13}$	93 021.503	2	411	43	6.2	–	–	–	–	–	–	–
$21_{5,17}-20_{5,16}$	93 022.018	2	369	43	6.9	–	–	–	–	–	–	–
$21_{5,16}-20_{5,15}$	93 022.027	2	369	43	6.9	–	–	–	–	–	–	–
$23_{0,23}-22_{0,22}$	100 963.335	2	352	47	9.3	141	0.025	100 962.2	100 965.1	6.7(5)⋆	5.2	5.5

Notes. See Table B.1.

Table B.7. Selection of lines of *gauche* propyl cyanide $v_{28} = 1$ covered by the EMoCA survey of Sgr B2(N2).

Transition[a]	Frequency (MHz)	Unc.[b] (kHz)	E_{up}[c] (K)	g_{up}[d]	A_{ul}[e] (10^{-5} s^{-1})	σ[f] (mK)	τ_{peak}[g]	Frequency range[h] (MHz)	(MHz)	I_{obs}[i] (K km s^{-1})	I_{mod}[j] (K km s^{-1})	I_{all}[k]
$15_{7,9}-14_{7,8}$	90 093.047	5	428	62	3.4	149	0.018	90 091.7	90 094.6	4.1(6)⋆	3.4	4.5
$15_{7,8}-14_{7,7}$	90 093.194	5	428	62	3.4	–	–	–	–	–	–	–

Notes. See Table B.1.

Table B.8. Selection of lines of *anti* propyl cyanide $v_{29} = 1$ covered by the EMoCA survey of Sgr B2(N2).

Transition[a]	Frequency (MHz)	Unc.[b] (kHz)	E_{up}[c] (K)	g_{up}[d]	A_{ul}[e] (10^{-5} s^{-1})	σ[f] (mK)	τ_{peak}[g]	Frequency range[h] (MHz)	(MHz)	I_{obs}[i] (K km s^{-1})	I_{mod}[j] (K km s^{-1})	I_{all}[k]
$21_{8,13}-20_{8,12}$	92 790.120	1	519	43	6.2	117	0.026	92 789.3	92 792.2	4.8(5)⋆	3.8	4.0
$21_{8,14}-20_{8,13}$	92 790.120	1	519	43	6.2	–	–	–	–	–	–	–
$21_{5,17}-20_{5,16}$	92 790.660	1	479	43	6.8	–	–	–	–	–	–	–
$21_{5,16}-20_{5,15}$	92 790.670	1	479	43	6.8	–	–	–	–	–	–	–

Notes. See Table B.1.